Title

Novel inhibitors of the cellular renin-angiotensin system components, poricoic acids, target Smad3 phosphorylation and Wnt/β-catenin pathway against renal fibrosis.

Journal

British journal of pharmacology, 175(13)

ISSN

0007-1188

Authors

Wang, Ming
Chen, Dan-Qian
Chen, Lin
et al.

Publication Date

2018-07-01

DOI

10.1111/bph.14333

Peer reviewed

JOURNAL OF AGRICULTURAL AND FOOD CHEMISTRY

Article

Novel RAS inhibitors poricoic acid ZG and poricoic acid ZH attenuate renal fibrosis via Wnt/#-catenin pathway and targeted phosphorylation smad3 signaling

Ming Wang, Dan-Qian Chen, Lin Chen, Hui Zhao, Dan Liu, Zhi-Hao Zhang, Nosratola D. Vaziri, Yan Guo, Ying-Yong Zhao, and Gang Cao

J. Agric. Food Chem., **Just Accepted Manuscript** • DOI: 10.1021/acs.jafc.8b00099 • Publication Date (Web): 31 Jan 2018

ACS Publications

Journal of Agricultural and Food Chemistry is published by the American Chemical Society. 1155 Sixteenth Street N.W., Washington, DC 20036

Novel RAS inhibitors poricoic acid ZG and poricoic acid ZH attenuate renal fibrosis via Wnt/β-catenin pathway and targeted phosphorylation smad3 signaling

Ming Wang[†,@], Dan-Qian Chen[†,@], Lin Chen[†], Dan Liu[†], Hui Zhao[†], Zhi-Hao Zhang[†], Nosratola D. Vaziri[‡], Yan Guo[†,§], Ying-Yong Zhao[*,†,‡], Gang Cao[*,$]

[†] Key Laboratory of Resource Biology and Biotechnology in Western China, Ministry of Education, School of Life Sciences, Northwest University, No. 229 Taibai North Road, Xi'an, Shaanxi 710069, China

[‡] Division of Nephrology and Hypertension, School of Medicine, University of California Irvine, Irvine, California 92897, USA

[§] Department of Internal Medicine, University of New Mexico, Comprehensive Cancer Center, Albuquerque, New Mexico, 87131, USA

[$] School of Pharmacy, Zhejiang Chinese Medical University, No. 548 Binwen Road, Hangzhou, Zhejiang 310053, China

[@] Both the authors contributed equally to the research.

Corresponding authors:

Professor Ying-Yong Zhao, PhD, MD

School of Life Sciences, Northwest University, No. 229 Taibai North Road, Xi'an, Shaanxi 710069, China, Tel: +86 29 88305273; Fax: +86 29 88303572, E-mail: zyy@nwu.edu.cn; zhaoyybr@163.com

Scientific Reports, American Journal of Nephrology, Editorial Board

Professor Gang Cao, PhD

School of Pharmacy, Zhejiang Chinese Medical University, No. 548 Binwen Road, Hangzhou, Zhejiang 310053, China; Tel/Fax: +86 571 87195895; E-mail: caogang33@163.com

ABSTRACT: Renal fibrosis is a common endpoint of the progression of chronic kidney disease (CKD). Suppressing the development and progression of renal fibrosis is essential in the treatment of kidney disease. Our previous study demonstrated that the ethyl acetate extract of the surface layer of *Poria cocos* exhibited beneficial anti-tubulointerstitial fibrosis. In this study, we isolated new diterpene (PZF) and triterpenes (PZG and PZH) and examined their anti-fibrotic effect. TGF-β1 upregulated the collagen I protein expression in HK-2 cells and PZG and PZH treatment significantly inhibited the upregulated collagen I expression (TGF group 0.59 ± 0.08 vs TGF+PZG group 0.36 ± 0.08, $P<0.01$; TGF+PZH group 0.39 ± 0.12, $P<0.01$). Triterpenes, PZG and PZH, exhibited a stronger inhibitory effect on renal fibrosis and podocyte injury than PZF. PZG and PZH further showed a stronger inhibitory effect on the activation of renin-angiotensin system (RAS) caused by renal injury than PZF. Additionally, PZG and PZH markedly inhibited the activation of Wnt/β-catenin signaling, which plays an important role in fibrogenesis. Interestingly, PZG and PZH suppressed TGF-β/Smad pathway by selectively inhibiting the phosphorylation of Smad3 through blocking the interactions of SARA with TGFβI and Smad3. The analysis of the structure-activity relationship demonstrated that the anti-fibrotic effect was closely associated with the first six-membered ring structure and the number of carboxyl groups in this type of compounds. These novel tetracyclic triterpenoid compounds provided the potential lead compounds for the research and development of anti-fibrosis drug and they possessed the potential to be utilized as RAS inhibitors.

KEYWORDS: Renin-angiotensin system; *Poria cocos*; poricoic acid; Wnt/β-catenin pathway; TGF-β/Smad pathway

■ INTRODUCTION

Renal fibrosis is the final pathways of progression of chronic kidney disease (CKD) to end stage renal disease (ESRD). The characteristic of renal fibrosis is the increase of myofibroblasts, inflammatory cells infiltration, and excessive extracellular matrix (ECM) accumulation in renal interstitium [1-3]. Renal fibrosis is closely related to TGF-β/Smad signaling pathway [4]. Transforming growth factor-β1 (TGF-β1) plays an irreplaceable role in the occurrence and the development of renal fibrosis. TGF-β1 is a potent cytokine that controls the transcription of many ECM genes. The

epithelial-mesenchymal transition (EMT), a critical process of tubulointerstitial fibrosis (TIF), is also driven by TGF-β1 [5, 6]. Smad is a significant downstream gene of TGF-β1 in the fibrogenesis. TGF-β1 leads to fibrogenic effect by the upregulation of Smad2 and Smad3 expression and the downregulation of Smad7 expression.

Renin-angiotensin system (RAS) and Wnt/β-catenin pathways also play an important role in renal fibrosis [7, 8]. All of the RAS components are present in the kidney tissues and activation of intrarenal RAS is a key component in the development and progression of renal fibrosis [9]. RAS consists of angiotensinogen (ATG), renin, angiotensin-converting enzyme (ACE), angiotensin II (Ang II), angiotensin II type 1 receptor (AT1) and angiotensin II type 2 receptor (AT2). Ang II is a key mediator in RAS-induced renal fibrosis. It stimulates TGF-β1 expression in the kidney, or directly phosphorylates Smad2 and Smad3 to promote fibrosis [10-12]. Although silent in adult kidney, Wnt/β-catenin is reactive after kidney injury. Wnt/β-catenin signaling induces renal fibrosis through promoting downstream target genes expression, most of which are fibrosis-related genes, including snail, twist, fibronectin, matrix metalloproteinase-7 (MMP-7), fibroblast specific protein-1 (Fsp-1), plasminogen activator inhibitor-1 (PAI-1) and RAS components [13]. Targeting inhibition of RAS/Wnt/β-catenin axis achieved better anti-fibrotic effect than targeting a single pathway, which indicated a new therapeutic strategy to mitigate renal fibrosis [8].

Recent studies demonstrated that small molecular weight natural products exhibited a good therapeutic effect on renal fibrosis [14-19]. Our previous studies showed that the ethanol extract of the surface layer of *Poria cocos* (SLPC) enhanced diuresis and was highly effective in the treatments of CKD [20, 21]. Further investigation indicated that the ethyl acetate extract of SLPC exhibited processes remarkable diuretic and anti-fibrotic effects [22-25]. In the present study, we investigated the renoprotective effect of three compounds with different skeletons isolated from the ethyl acetate extract of SLPC. The three newly found and reported compounds include one new diterpene poricoic acid ZF (PZF) and two new triterpenes poricoic acid ZG (PZG) and poricoic acid ZH (PZG). TGF-β1 and Ang II were used to stimulate HK-2 cells and podocytes to induce renal injury. The treatment with PZF, PZG and PZH inhibited renal fibrogenesis, and the

anti-fibrotic effect of PZF, PZG and PZH were mediated by the suppression of RAS, TGF-β/Smad3 and Wnt/β-catenin signaling pathways.

■ MATERIALS AND METHODS

Chemicals and Instruments. HPLC-grade methanol and acetonitrile was purchased from Baker Company (Baker Inc., USA). AR grade methanol, ethanol and acetonitrile were purchased from Tianjin Guangfu Fine Chemical Research Institute (Tianjin, China). Chemicals were purchased from Thermo Fisher Scientific (New York, USA), unless indicated otherwise. Ultra high purity water (UHP) was prepared by a Millipore-Q (France). DMEM-F12, DMEM and fetal bovine serum were purchased from Gibco (Carlsbad, USA). Lipofectamine RNAiMAX was purchased from Invitrogen (New York, USA). The recombinant human TGF-β1 protein and recombinant human ANG II protein were purchased from R&D system (New York, USA). The losartan (LOS) was purchased from Selleck (Shanghai, China). Other chemicals were of analytical grade and their purity was above 99.5%.

Infrared (IR) spectrum was analyzed by using a Perkin Elmer FTIR system and Spectrum 2000 spectrophotometer (Perkin Elmer, USA). ^{1}D and ^{2}D NMR spectra were measured by using Bruker AM-500 spectrometer (Bruker, Zurich, Switzerland) with TMS as an internal standard. HRESI/MS were tested by an Agilent high-performance liquid chromatography (HPLC)-Thermo Finnigan LCQ Advantage ion trap mass spectrometer (California, USA). Column chromatography was carried out on silica gel (200-300 mesh, Qingdao Marine Chemical Inc., Shandong China). HPLC analysis and purification were performed on a Hanbon HPLC system equipped with a NP7000C serials pump and a NU3000 serials detector (Hanbon, Jiangsu, China) at 210 nm, and the column used was a YMC-Pack C_{18} column (250 mm× 4.6 mm i.d., 5 μm).

Materials, extraction and isolation. SLPC were collected in Yunnan Province (China) and authenticated by Fang M. F. (Northwest University). The voucher specimen (16-09-12-01) was deposited in the herbarium of School of Life Sciences, Northwest University. The dried and powdered SLPC (20 kg) was extracted with 95% ethyl alcohol (100 L × 3) three times with at room temperature. The filtrates were combined and concentrated under reduced pressure until

92 elimination of ethyl alcohol to obtain crude extracts. Crude extracts (204 g) was fractionated by silica gel column
93 chromatography (60 × 10 cm) with the use of a gradient solvent system of $CHCl_3$/MeOH (from 100:0 to 1:1) to give six
94 fractions (FL1-FL6) according to TLC analysis. Fraction FL2 (12.0 g) was subjected to column chromatography using
95 silica gel with $CHCl_3$-MeOH (97:7) as a solvent system, and PZF (9 mg) was obtained. Fraction FL5 (24.1 g) was
96 fractionated by silica gel column chromatography with the use of a gradient solvent system of $CHCl_3$-MeOH (from 10:1
97 to 1:1) to obtain four fractions. The FL5-2 (2.7 g) was purified over reversed-phase HPLC with a gradient of
98 MeOH-H_2O (79:21 to 83:17 v/v) to yield PZG (7 mg, tR=17.2 min). Fraction FL5-3 (1.3 g) was further purified over
99 reversed-phase HPLC (MeOH-H_2O, 75:25) to obtain PZH (6 mg, tR=15.4 min).

100 **Cell culture and treatment.** Human kidney proximal epithelial cells (HK-2) and conditionally immortalized mouse
101 podocytes (MPC5) were employed to test the anti-fibrotic effect of PZF, PZG and PZH on Ang II and TGF-β1
102 stimulation. HK-2 cells were cultured in DMEM-F12 supplemented with 10% fetal bovine serum, and MPC5 was
103 cultured in DMEM containing 5.5 mM glucose with 10% fetal bovine serum. HK-2 cells were grown at 37°C with
104 5% CO_2, while MPC5 were grown at 33°C and differentiated at 37°C with 5% CO_2. The concentration of recombinant
105 human TGF-β1 protein was 2.5 ng/ml, and the concentration of recombinant human ANG II protein was 1.0 μM. The
106 10 μM of PZF, PZG and PZH were used to treat Ang II and TGF-β1-stimulated cells. The 10 μM of LOS was used to
107 treat HK-2 and MPC5. The cell viability of PZF, PZG and PZH were detected by CCK-8.

108 **Analysis of cell viability by CCK-8.** CCK-8 kit was purchased from EnoGene (Shanghai, China). The 1×10^4 cells
109 were cultured in 96-well plates and treated with different concentrations of ZF, PZG and PZH (0, 1, 10, 50, 100 μM) for
110 24 hours. Before added 10 μl CCK-8, 100 μl/well fresh medium was added into plates. After 3 hours incubation, the
111 absorbance was detected at 450 nm on a microplate reader (Thermo, New York, USA). Six repeats were employed to
112 determine the cell viability of each concentration.

113 **Knockdown of Smad3 by siRNA.** HK-2 cell lines were grown to 60% confluence and the siRNA targeting human
114 Smad3 (5'-CCGCAUGAGCUUCGUCAAATT-3') and negative control (5'-UUCUCCGAACGUGUCACGUTT-3')

were transfected with 3μl of 10 μM siRNA/well. Lipofectamine RNAiMAX was employed. The transfected cells were measured by Western blot and qRT-PCR.

Gene expression studies by qRT-PCR. Total RNA was isolated using a High Pure RNA Isolation Kit (Tokyo, Japan) according to the manufacturer's protocol. Total RNA was used for reverse transcription by a Transcriptor First Strand cDNA Synthesis Kit (Roche, Germany). Real time quantifications of target genes were assessed using SYBR® Premix Ex Taq™ II (Takara Bio, Japan). The housekeeping gene β-actin was used as the endogenous control. Samples were amplified with a precycling hold at 95˚C for 30 seconds, 30 cycles of annealing and extension at 60 ˚C for 30 seconds by using BioRad CFX 96 Touch™ system (Bio-Rad, USA).

Western blot analysis. Protein expression was performed by Western blot analysis as described previously [26, 27]. Cells were lysed in RIPA lysis buffer. Protein levels were measured by BCA Protein Assay Kit (23227, Thermo Scientific, USA) and normalized by immunoblotting with α-tubulin, GAPDH or histone H3 expression. Total protein was separated by SDS/PAGE and transferred to PVDF membranes (10600023, Amersham™ Hybond™, GE Healthcare, USA). Membranes were blocked in 1×TBS with 0.1% Tween-20 (TBST) with 5% non-fat milk and then were incubated with the primary antibodies. Finally, membranes were washed, incubated with goat anti-rabbit (1:5000, ab6721, Abcam, USA), goat anti-mouse (1:5000, A21010, Abbkine, USA) or rabbit anti-goat (1:5000, A21110, Abbkine, USA) secondary antibodies, and developed with ECL (RPN2232, GE Healthcare, USA).

The following primary antibodies were employed (dilution): AGT (1:200, sc-7419, Santa Cruz Biotechnology, CA), renin (1:2000, 14291-1-AP, Proteintech, China), ACE (1:1000, sc-23908, Santa Cruz Biotechnology, CA), AT1 (1:800, ab124505, Abcam, USA), Wnt1 (1:1000, ab85060, Abcam, USA), dephosphorylated active non-phosphorylated β-catenin (1:2000, 05-665, Millipore, USA), β-catenin (1:1000, 610154, BD Transduction Laboratories, USA), collagen I (1:5000, ab34710, Abcam, USA), alpha smooth muscle actin (α-SMA, 1:300, ab7817, Abcam, USA), fibronectin (1:1000, ab2413, Abcam, USA), Snail1 (1:1000, ab180714, Abcam, USA), MMP-7 (1:400, ab5706, Abcam, USA), Twist (1:2000, ab50581, Abcam, USA), Fsp-1(S100A4, 1:1000, ab197896, Abcam, USA), transforming growth factor

β receptor I (TGFβRI, 1:1000, ab31013, Abcam, USA), transforming growth factor β receptor II (TGFβRII, 1:2000, ab186838, Abcam, USA), Smad2 (1:2000, 5339, CST, USA), p-Smad2 (1:2000, 3180, CST, USA), Smad3 (1:2000, 9523, CST, USA), p-Smad3 (1:2000, 9520, CST, USA), Smad4 (38454, CST, USA), Smad7 (1:500, sc-365846, Santa Cruz, USA) and α-tubulin (Proteintech Company, China).

Immunofluorescence staining. Indirect immunofluorescence staining was performed using an established procedure [8]. HK-2 cells were cultured on coverslip, and then fixed with fresh 4% paraformaldehyde solution. Normal goat serum was used to reduce non-specific background staining. Cells were stained with primary antibody followed by treatment with Alexa Fluor® 488 or 594-conjugated secondary antibody (Abcam, USA) for visualization. DAPI was employed to localize nuclear. Cells were visualized by using a laser-scanning confocal microscope (FV1000, Olympus, Japan) with FV10-ASW 4.0 VIEW.

Co-immunoprecipitation (CO-IP) analysis. After various treatments, HK-2 cells and podocytes were lysed by M-PER™ Mammalian Protein Extraction Reagent (78501, Thermo Scientific, USA). After preclearing with protein A/G (Immunoprecipitation Starter Pack, GE Healthcare, USA), cell lysates were incubated with anti-TGFβRI (1:100), anti-Smad2 (1:100) and anti-Smad3 (1:100) antibody overnight at 4°C, and then precipitated with protein A/G overnight at 4°C. The precipitated complexes were analyzed by western blotting.

Statistics analysis. All results were analyzed as means ± SD. GraphPad Prism software v 5.0 (San Diego, USA) was used to calculate the statistical differences among different groups by one-way ANOVA. *P* values smaller than 0.05 were considered as statistically significant.

■ RESULTS

Structure elucidation of isolated new compounds (PZF, PZG, PZH).

In this study, we isolated three novel compounds (PZF-PZH) from *P. cocos*. PZG and PZH were two novel triterpenes, and PZH was found to possess a unique 5(6),8(9)-diene at B/C rings, all of which was identified for the first time in triterpenes isolated from *P. cocos* **(Figure 1)**. PZF was isolated as a yellow, amorphous powder. Its molecular formula,

$C_{30}H_{46}O_3$, was determined by HRESIMS molecular ion at m/z 453.1669 $[M-H]^-$ and ^{13}C NMR data. Its IR spectrum revealed the absorption bands of the aliphatic long-chain (2924 cm-1), carbonyl (1711 cm-1) and aromatic ring (1639, 1449 cm-1) groups. The ^1H NMR spectrum of PZF indicated the presence of three protons in a trisubstituted aromatic ring at δ_H 7.29 (d, J = 8.2 Hz), 7.12 (dd, J = 8.1, 1.8 Hz) and 6.95 (d, J = 1.3 Hz); two quaternary methyl groups at δ_H 1.49 and 1.21; two singlet methyl groups both at δ_H 1.23. The ^{13}C DEPT spectra of PZF revealed 30 carbon resonances, belonging to five methyls, 12 methylenes, six methines, and seven aromatic/olefinic quaternary carbons. According to the ^{13}C NMR spectrum, there were the typical signals of one carbonyl carbon at δ_C 176.4 corresponding to C-18, one carboxyl carbon at δ_C 184.1 corresponding to C-20, and an isopropyl carbons at δ_C 34.3, 24.6 and 24.6 corresponding to C-15, C-16 and C-17, respectively. A chain structure from C-1' to C-9' connected with C-18 was confirmed by the important connectivities found in the heteronuclear multiple-bond connectivity (HMBC) spectrum (as shown in **Figure 1**) from H-19 (δ_H 1.49) to C-1' (δ_C 37.8), and from H-5 (δ_H 2.55) to C-18 (δ_C 176.4), and from H-1' (δ_H 1.84) to C-18 (δ_C 176.4). Furthermore, the HMBC signals from H-16, 17 (δ_H 1.23) to C-13 (δ_C 146.3) revealed that C-13 was connected with the isopropyl group. The relative stereochemistry of PZF was assessed by its nuclear overhauser effect pectroscopy (NOESY) spectrum (Fig. 1). The interactions between Me-19 (δ_H 1.49) and the protons at Me-21 (δ_H 1.21) revealed that they were on the same side of the molecule, while the nuclear Overhauser effect (NOE) between H-2 (δ_H 1.41) and H-5 (δ_H 2.55) suggested that Me-30 and H-18 were on the same side. All of these data established the structure of PZF as abieta-8,11,13-trien-18-pelargonyl-2-oic acid.

PZG was obtained as a white, amorphous powder. Its HRESIMS molecular ion at m/z 525.3176 $[M+Na]^+$ and ^{13}C NMR data were consistent with the molecular formula $C_{30}H_{46}O_6$ (calcd 525.3192). The IR spectrum indicated the presence of OH and C=C functional groups based on the absorptions at 3430 and 1644 cm^{-1}, respectively. The ^1H NMR data (Table 1) showed six methyls at δ_H 1.05 (s), 1.11 (s), 1.36 (s), 1.36 (s), 1.51 (s) and 1.75 (s), two olefinic protons at δ_H 5.30 (t) and 5.36 (br s), and an olefinic methylene at δ_H 4.85 (s) and 4.78 (s). The ^{13}C NMR data (Table 2) revealed 30 carbon signals sorted by HSQC and DEPT. They included two carboxylic carbon at δ_C 177.0 and 179.2, six olefinic carbons at

184 δ_C 149.7, 142.3, 138.0, 120.8, 118.4 and 112.6, and one oxymethine carbon at δ_C 76.8.These data suggested that PZG
185 belonged to the group of 3,4-seco-lanostan-7,9(11)-diene type triterpenes. The hydroxyl group was located at C-25,
186 which was supported by the correlation from H-26, 27 (δ_H 1.36) to C-25 (δ_C 70.0), and from H-23 (δ_H 1.89) to C-25 (δ_C
187 70.0) in the HMBC experiment. The relative stereochemistry of PZG was assessed by its NOESY spectrum (Fig. 1).
188 The NOESY cross peaks of H-16 (δ_H 4.53) and Me-18 (δ_H 1.11), as well as interactions between H-16 (δ_H 4.53) and
189 H-20 (δ_H 2.98) suggested the α-orientation assignments of OH-16. Therefore, PZG was identified as
190 (20R)-16α,25-dihydroxy-3,4-seco-lanosta-4(28),7,9(11)-triene-3,21-dioic acid.
191 PZH was isolated as a white amorphous powder. It gave a $[M+Na]^+$ ion in the HRESIMS at m/z 521.3226, which was
192 consistent with a molecular formula of $C_{31}H_{46}O_5$ (calcd 521.3243). The IR spectrum indicated the presence of OH
193 (3430 cm^{-1}) and C=C (1650 cm^{-1} and 1644 cm^{-1}) functional groups. The ^1H NMR spectrum had seven methyls signals
194 at δ_H 1.64 (3H, s, Me-30), 1.41 (3H, s, Me-28), 1.38 (3H, s, Me-19), 1.34 (3H, s, Me-29), 1.17 (3H, s, Me-18), 1.01 (3H,
195 s, Me-27) and 1.00 (3H, s, Me-26), one olefinic proton at δ_H 6.56 (1H, s, H-6), and an olefinic methylene at δ_H 5.02 (s)
196 and 4.87 (s). The ^{13}C DEPT and ^1H NMR data and IR spectra of PZH indicated the presence of seven methyls, eight
197 methylenes, six methines and ten quaternary carbons (including one carboxylic carbon at δ_C 179.5 corresponding to
198 C-21). The presence of a tetrasubstituted double bond at C-8 and C-9 was supported by the correlation from H-30 (δ_H
199 1.64) to C-8 (δ_C 140.1), and from H-19 (δ_H 1.38) to C-9 (δ_C 162.9) in the HMBC experiment **(Figure 1)**. Besides, the
200 correlation between H-29 (δ_H 1.34), H-19 (δ_H 1.38), H-28 (δ_H 1.41) and C-5 (δ_C 186.6), as well as the correlation
201 between H-6 (δ_H 6.56) and C-8 (δ_C 140.1) in the HMBC experiment suggested the location of a trisubstituted double
202 bond at C-5 and C-6. The NOESY cross peaks of H-16 (δ_H 4.48) and Me-18 (δ_H 1.17), as well as interactions between
203 H-16 (δ_H 4.48) and H-20 (δ_H 2.96) suggested the α-orientation assignments of OH-16. The ^{13}C NMR data of C-3 (δ_C
204 77.4) suggested the OH-3 was α-orientation, and it was supported by interactions between δ_H 4.60 (H-3) and δ_H 1.34
205 (H-29) in the NOESY experiment (Fig. 1). Hence, the structure of PZH was proposed as
206 (20R)-3α,16α-dihydroxy-7-oxo-24-methyllanosta-5(6),8(9),24(31)-trien-21-oic acid.

The toxicity of PZF, PZG and PZH on HK-2 cells. To test the toxicity of PZF, PZG and PZH, the 0, 1, 10, 50 and 100 μM of PZF, PZG and PZH were incubated with HK-2 cells, respectively. CCK-8 method was used to test the value of cell viability after 24 hours incubation. The values of cell viability were 0.98±0.06, 0.99±0.05, 0.99±0.03, 1.03±0.06 and 1.05±0.03 after incubation with the concentrations of 0, 1, 10, 50 and 100 μM of PZF, respectively. The values of cell viability were 1.03±0.04, 0.99±0.05, 1.02±0.03, 0.98±0.09 and 1.00±0.07 after incubation with the concentrations of 0, 1, 10, 50 and 100 μM of PZG, respectively. The values of cell viability were 1.02±0.03, 0.99±0.05, 0.98±0.04, 1.01±0.02 and 1.00±0.06 after incubation with the concentrations of 0, 1, 10, 50 and 100 μM of PZH, respectively. In conclusion, PZF, PZG and PZH showed no toxicity on HK-2 cells. The 10 μM of PZF, PZG and PZH was used for subsequent experiments.

PZF, PZG and PZH attenuated TIF and podocyte injury induced by TGF-β1 and Ang II. Collagen I, as one of most important component of fibrosis, is an important indicator in renal fibrosis, so we chose collagen I as an indicator for the determination of the inhibitory effect of the different concentrations of PZF, PZG and PZH in the TGF-β1-induced HK-2 cells. The compound concentrations of 1, 10, 50 and 100 μM were tested for collagen I protein expression in HK-2 cells by induced TGF-β1. As shown in **Figure 2A,** the concentration of 10 μM PZF, PZG and PZH exhibited a strong anti-fibrotic effect. Hence, we selected the 10 μM of PZF, PZG and PZH for the subsequent experiments.

We investigated the inhibitory effect of PZF, PZG and PZH on ECM accumulation, which was mainly expressed by myofibroblasts. TGF-β1 directly accumulates transcription of many ECM genes in HK-2 cells. Ang II directly stimulates the expression of TGF-β1, and directly stimulates Smads to induce renal fibrogenesis. In this study, both TGF-β1 and Ang II significantly upregulated the expression of ECM, including collagen I, fibronectin and α-SMA **(Figure 2B-E)**. E-cadherin is an epithelial cell marker and controls cell-cell junctions [28]. E-cadherin can be viewed as an inhibitor of EMT [29]. The protein expression of E-cadherin was significantly downregulated in HK-2 cells by inducing TGF-β1 or Ang II **(Figure 2B-E).** The dysregulation caused by TGF-β1 and Ang II were reversed by

triterpene PZG and PZH, but diterpene PZF hardly changed the dysregulation **(Figure 2B-E)**. The upregulated mRNA expressions of collagen I, fibronectin, α-SMA and vimentin were suppressed by PZG and FZH, while downregulating E-cadherin mRNA expression induced by TGF-β1 was reversed **(Figure 2F)**. Interestingly, PZG exhibited a stronger inhibitory effect than PZH. Additionally, immunofluorescent staining also showed that upregulated vimentin expression were inhibited by PZG and PZH, whereas the expression of vimentin showed no fluctuation after given PZF, PZG or PZH alone **(Figure 2K)**.

Next, we explored the protective effect of PZF, PZG and PZH on podocyte injury. TGF-β1 and Ang II stimulation resulted in podocyte injury. The expression of podocyte-specific proteins, including podocin, nephrin, podocalyxin and synaptopodin, were significantly decreased after TGF-β1 or Ang II stimulation **(Figure 2G-J)**. Triterpene compounds PZG and PZH, rather than diterpene compound PZF, exhibited a protective effect on podocyte injury **(Figure 2G-J)**. In conclusion, triterpene PZG and PZH showed a good therapeutic effect on TIF and podocyte injury. The different effects among triterpene compounds PZG, PZH and diterpene compound PZF were caused by the differences in the chemical structures. Our results indicated that triterpene was the active compound of SLPC in the treatment of renal fibrosis and podocyte injury. Interestingly, compared with the PZH, PZG showed stronger inhibitory effect on the TGF-β1- and Ang II-induced TIF and podocyte injury. The loss of first intact six-membered-ring led to hydroxyl group in PZH transforming into carboxyl group in PZG. The increasing number of carboxyl group may be associated with the bioactivity of triterpene compound.

PZF, PZG and PZH inhibited the activation of RAS. Since the inhibition of activated RAS was beneficial to treatment of renal fibrosis and CKD [30, 31], we examined the suppression of PZF, PZG and PZH on the activation of RAS induced by TGF-β1 and Ang II. TGF-β1 stimulation upregulated the protein expression of RAS components in HK-2 cells. After PZG and PZH treatment, activated RAS was inhibited, while PZF showed no effect on activated RAS **(Figure 3A,B)**. Similarly, PZG and PZH significantly suppressed the activation of RAS caused by Ang II, while the inhibitory effect of PZF was weak **(Figure 3C,D)**. Next, we examined the inhibitory effect of PZF, PZG and PZH on

activated RAS in podocyte. TGF-β1 stimulation activated RAS, and the expressions of RAS components were increased. The significant decrease of RAS components were observed after PZG and PZH treatment, especially for ACE and AT1 **(Figure 3E,F)**. PZG and PZH were also obviously decreased abnormal activated RAS caused by Ang II, whereas PZF showed a weak regulatory effect on this abnormality **(Figure 3G,H)**.

PZF, PZG and PZH suppressed activated Wnt/β-catenin and its downstream target genes expression. Wnt/β-catenin signaling is closely related to renal disease, especially for renal fibrosis [32]. Both TGF-β1 and Ang II stimulated the activation of β-catenin and the transcription of downstream target genes, resulting in upregulation of downstream target genes. PZG and PZH significantly inhibited the upregulation of Wnt1, β-catenin, active non-phosphorylated β-catenin, snail1, twist, MMP-7, PAI-1 and Fsp-1 expression induced by TGF-β1 and Ang II. However, PZF had no effect on Wnt/β-catenin expression **(Figure 4A-D)**. PZG and PZH also significantly inhibited the upregulated mRNA expression of Wnt1, Wnt2, Wnt3, Wnt3a, Wnt7a and Wnt8a **(Figure 4E)**. Immunofluorescent staining also showed that PZG and PZH treatment have a significantly inhibitory effect on the β-catenin expression in HK-2 cells induced by TGF-β1 **(Figure 4F)**. PZG and PZH performed better than PZF on the suppression of activated Wnt/β-catenin in renal epithelial cell. In podocyte, PZG and PZH attenuated the upregulating protein expression of Wnt1, β-catenin and active β-catenin induced by TGF-β1 and Ang II, and the increase of target genes, such as snail1, twist, MMP-7, PAI-1 and Fsp-1, were reversed by PZG and PZH in podocytes **(Figure 4G-J)**. PZG and PZH suppressed the activation of Wnt/β-catenin in HK-2 cells and podocytes.

PZF, PZG and PZH selectively inhibits TGF-β/Smad3 pathway. Since TGF-β/Smad signaling played an irreplaceable role in the development and progression of renal fibrosis, we examined several important proteins in this pathway. We found that TGF-β1 and Ang II significantly induced the expressions of TGFβRII, p-Smad2, p-Smad3 and Smad4, and significantly reduced Smad7 expression, which indicated activation of TGF-β/Smad signaling induced by TGF-β1 and Ang II. TGF-β1 or Ang II promoted the phosphorylation of Smad2 and Smad3 and upregulated the expression of p-Smad2 and p-Smad3, but did not change the expression of total Smad2 and Smad3. After PZH and PZG

treatment, the upregulation of p-smad3 was significantly inhibited. PZH and PZG only mitigated the upregulation of p-Smad3, but showed no effect on the dysregulation of p-Smad2, Smad2, Smad3, Smad4 and Smad7 in HK-2 cells, indicating Smad3 might be the intervention target of PZH and PZG **(Figure 5A-D)**. Immunofluorescence staining results demonstrated that PZH and PZG showed a stronger inhibitory effect on p-Smad3, but PZF have no effect on p-Smad3 **(Figure 5E)**. Similar results were observed in podocyte. TGF-β1 and Ang II significantly upregulated p-Smad2 and p-Smad3, but PZH and PZG treatment only inhibited the upregulation of p-Smad3 **(Figure 5F-I)**. PZH and PZG specifically attenuated increased p-Smad3 in HK-2 cells and podocytes, indicating PZH and PZG suppressed the phosphorylation of Smad3 induced by TGF-β1 and Ang II.

PZF, PZG and PZH selectively interrupt the interactions of Smad3 with TGFβRI and SARA. To further explore the changes within TGF-β/Smad pathway, CO-IP were employed. First, we explored the interactions of TGFβRI and Smad2/3, founding that PZG and PZH only disturbed the interaction between TGFβRI and p-Smad3 **(Figure 6A,B)**. The interactions of Smad2 with TGFβRI and TGFβRII was unaltered after PZF, PZG and PZH treatment **(Figure 6C,D)**. Of note, PZG and PZH significantly weakened the interactions of Smad3 with TGFβRI and TGFβRII **(Figure 6E,F)**. These results suggested that PZG and PZH specifically affected the interactions of Smad3 with TGFβRI and TGFβRII, instead of Smad2.

Since after TGF-β1 stimulation, TGFβRI and Smad2/3 were connected by adaptor proteins such as Smad anchor for receptor activation (SARA) [33, 34], we explored the interactions of SARA with TGFβRI and Smad2/3. The interaction of Smad3 with SARA was obviously weakened by PZG and PZH treatment, but PZG and PZH performed no effect on the interaction of Smad2 with SARA **(Figure 6G-J)**. As shown in **Figure 6K**, PZG and PZH specifically affected the interaction between SARA and Smad3 to suppress the phosphorylation of Smad3 and downregulated the expression of p-Smad3. These results indicated that Smad3 was the intervention target of PZF and PZH for suppressing TGF-β/Smad pathway and retard renal fibrosis.

PZF, PZG and PZH performed no anti-fibrotic effect after knockdown of Smad3. According to our results, Smad3 was the main target of PZG and PZH to retard renal fibrosis. Specific Smad3 siRNA was employed to further confirm the mechanism of PZG and PZH. We hypothesized that Smad3 was the primary target of PZG and PZH, which could explain the results that once Smad3 decreased, PZG and PZH lost the intervention target and thus showed no effect on renal fibrosis. First, we examined the inhibitory effect of specific Smad3 siRNA, founding that the protein expression of Smad3 was significantly downregulated in HK-2 cells induced by specific Smad3 siRNA **(Figure 7A)**. Moreover, PZF, PZG and PZH had no influence on the process of RNAi, and would not upregulate Smad3 protein expression **(Figure 7B)**. Interestingly, after knockdown Smad3, the anti-fibrosis of PZG and PZH significantly weakened, which provided the evidence that Smad3 was the main intervention target of PZG and PZH to mitigate renal fibrosis **(Figure 7C,D)**.

Structure-activity correlation of PZF, PZG and PZH. Our study demonstrated that PZG exhibited a stronger inhibitory effect on the TGF-β1- and Ang II-induced excessive ECM accumulation in HK-2 cells than PZH. According to the classification of compound chemical structure, PZG and PZH belonged to secolanostane tetracyclic triterpenoid compound and lanostane tetracyclic triterpenoid compound, respectively. The most important difference of two tetracyclic triterpenoid compounds is that the first six-membered ring in the secolanostane compounds is opening-ring chemical structure, but the first six-membered ring in lanostane compounds was intact six-membered ring chemical structure. The loss of first intact six-membered-ring led to hydroxyl group in PZH transformed into carboxyl group in PZG. Increasing number of carboxyl group may be associated with the bioactivity of triterpene compound. This result indicated that compound skeleton has an important effect on this type of secolanostane and lanostane tetracyclic triterpenoid compounds.

We compared the chemical structures of PZF and PZG. PZF and PZG both had chemical structures of three-membered ring and one carboxyl group in the parent nucleus. PZF had no inhibitory effect on TGF-β1- and Ang II-induced cell injury, but PZG showed an inhibitory effect on TGF-β1- and Ang II-induced cell injury. This result indicated that carboxyl group in PZG plays a crucial role in this type of compound.

■ DISCUSSION

Natural products have been widely used for the treatment of CKD and inhibition of renal fibrosis [35-38]. Our previous study demonstrated that SLPC exhibited a good therapeutic effect on CKD. The ethanol extract of SLPC ameliorates adenine-induced CKD by correcting the disturbance of amino metabolism and fatty acid metabolism [22-24]. On the basis of biological activity screening, the ethyl acetate extract is the main active fraction. Diterpene compound PZF and triterpene compounds PZG and PZH were isolated from SLPC. In the present study, we found that PZG and PZH significantly attenuated renal fibrosis caused by inducing TGF-β1 and Ang II. PZG and PZH exert their effect by targeting the phosphorylation of Smad3, through inhibiting the interactions of Smad3 with TGFβRI with SARA. PZG and PZH exhibited a strong inhibitory effect on the activation of RAS and Wnt/β-catenin signalings **(Figure 8)**. However, PZF showed a weak effect, indicating triterpene components were the active component of SLPC, instead of diterpene components. These important bioactivities may be associated with the first six-membered ring and the number of carboxyl groups in secolanostane and lanostane tetracyclic triterpenoid compounds. This study provided activity targets for anti-fibrosis drug research and development.

Regardless of the type of initial injury to the kidney, renal fibrosis is the common final pathway of CKD to ESRD [39]. The accumulation of ECM in the region between peritubular capillaries and tubules suppresses tubular function. ECM resulted in tubules injury, tubular necrosis and interstitial fibrosis. Fibrosis in glomerular led to reduced filtration and the loss of blood flow [40]. With the increasing renal fibrosis area, the structural support of kidney was lost and kidney volume was decreased, which led to the loss of renal function. Suppression the development and progress of renal fibrosis is an indispensable component in CKD treatment. PZG and PZH showed excellent inhibitory effects on the increase expression of collagen I, fibronectin, α-SMA and the decrease expression of E-cadherin, but PZF had no influence on the dysregulation. Collagen I is an important component of fibrosis, and the decrease of collagen I is a vital parameter to measure the anti-fibrotic effect. Fibronectin is the component of ECM, and PZG and PZH inhibited fibronectin expression caused by inducing TGF-β1 and Ang II in HK-2 cells and podocytes. α-SMA, the marker of

myofibroblasts, is mainly expressed in interstitium. After PZG and PZH treatment, α-SMA was downregulated, which indicated the inhibition of EMT. PZG and PZH exhibited a good anti-fibrotic effect, and this may involved in several signaling pathways, including RAS, TGF-β/Smad and Wnt/β-catenin signaling.

RAS controls the blood pressure and fluid balance, and the activation of RAS is the major cause of hypertensive nephropathy [41]. CKD caused hypertension and hypertension further activated RAS [42]. RAS inhibitors, especially for angiotensin-converting enzyme inhibitor (ACEI) and angiotensin II type 1 receptor blocker (ARB), were the first-line therapy for CKD. ACEI and ARB antagonize Ang II to treat CKD. Ang II is a key mediator in RAS-induced renal fibrosis [43]. It stimulates TGF-β1 and Smads to promote renal fibrogenesis [5]. TGF-β1 and Ang II induce the activation of RAS, while PZG and PZH suppress the activation of RAS by downregulating the expression of AGT, renin, ACE and AT1. Our study provides strong evidence that PZG and PZH are novel RAS inhibitors.

Wnt/β-catenin signaling pathway is an evolutionarily conserved signaling pathway that is regulated by the amount of β-catenin [44]. Wnt/β-catenin is silent in adult kidney tissue. However, Wnt/β-catenin is reactivated in injured kidney, especially in CKD [7, 45]. Wnt/β-catenin plays an opposite role in CKD compared to the RAS. Wnt/β-catenin is advantageous in acute kidney injury for the restoration of kidney morphology and function [46], but harmful in CKD [47]. The continuous activation of Wnt/β-catenin drives acute kidney injury to CKD [46]. The upregulation of Wnt1 ligand, active β-catenin and β-catenin were observed after TGF-β1 and Ang II stimulation, which indicated the activation of Wnt/β-catenin pathway. PZG and PZH efficiently suppressed activated Wnt/β-catenin and its downstream target gene expression. Upregulation of downstream target genes promoted renal fibrosis [8]. Snail is a key transcription factor of EMT and facilitates fibroblast migration, and was downregulated by PZG and PZH. MMP-7 is the component of ECM and mediates the degradation of E-cadherin. MMP-7 was significantly inhibited by PZG and PZH. PAI-1 recruits myofibroblasts, and PAI-1 was significantly inhibited by PZG and PZH. The expression of fibrotic marker, Fsp-1, was also attenuated by PZG and PZH. PZG and PZH were better in the suppression of Wnt/β-catenin and its downstream target gene expression than PZH.

Undoubtedly, TGF-β/Smad plays a central and dominant role in the initiation and development of renal fibrosis [48-50]. The TGF-β isoforms spread all over every cell type in mammals. The ubiquitous intracellular signaling cascade Smad family protein is the major pathway of TGF-β signaling in renal fibrogenesis. The active TGF-β1 binds to TGFβRII, then recruits and phosphorylates TGFβRI, which results in the phosphorylation of Smads [51]. The binding between TGFβRI and Smads is mediated by adaptor proteins, including SARA. Among several Smads, Smad3 is recognized as the most important one during fibrogenesis [10, 14], which directly connected with promoter region of collagens to trigger their production [52]. Smad7 is negative regulator of TGF-β/Smad signaling, and the expression of Smad7 is significantly downregulated in CKD. The expression of Smad7 is a Smad3-dependent mechanism, and suppresses TGF-β1 in turn [53]. Activated Smad protein complexes transfers into the nucleus and engage the transcription of target genes [54]. In the present study, we tested the expression of primary proteins, and found that PZH and PZG inhibited the upregulation of p-Smad3 expression specifically, which indicated the phosphorylation of Smad3 were suppressed. CO-IP showed that After PZG and PZH treatment, the binding between TGFβRI and Smad3 was weak. Since TGFβRI phosphorylated Smad3 by the connection of SARA, the suppressed phosphorylation of Smad3 may result in broken connection. The interaction of SARA with TGFβRI and Smad3 were simultaneously suppressed. Interestingly, PZG and PZH had no effect on the phosphorylation of Smad2 and the interactions of SARA with TGFβRI and Smad2. In conclusion, PZG and PZH targeted the phosphorylation of Smad3 by inhibiting the connection of SARA with TGFβRI and Smad3 in the TGF-β/Smad pathway. When the expression of Smad3 subsided, PZG and PZH lost the intracellular target. This provided potent evidence for elucidating anti-fibrotic mechanism of PZG and PZH.

In this study, we isolated the active components of renoprotective effect of SLPC and elucidated their anti-fibrotic mechanism. Triterpenes, PZG and PZH, are the major active components of SLPC to treat retard renal fibrosis, instead of diterpene PZF. PZG and PZH exhibited a stronger anti-fibrotic effect than PZF though inhibiting RAS, Wnt/β-catenin and TGF-β/Smad signaling pathways. PZG and PZH demonstrated strong potential to be developed as new RAS inhibitors. PZG and PZH specifically inhibited the phosphorylation of Smad3 and mitigated renal fibrosis.

The anti-fibrotic effect is closely associated with the first six-membered ring structure and the number of carboxyl groups in tetracyclic triterpenoid compounds. This study provides novel intervention targets for the development of effective anti-fibrotic agent.

Corresponding Author

*(Y.-Y.Z.) Tel: +86-29-88305273. Fax: +86-29-88303572. E-mail: zyy@nwu.edu.cn, zhaoyybr@163.com. (G.C.) Phone: +Tel/Fax: +86 571 87195895; E-mail: caogang33@163.com

Funding

This study was supported by the National Natural Science Foundation of China (Nos. 81673578, 81603271).

Notes

The authors declare that there is no conflict of interest.

■ ABBREVIATIONS USED

ACE, angiotensin-converting enzyme; ACEI, angiotensin-converting enzyme inhibitor; AGT, angiotensinogen; AngII, angiotensin II; ARB, angiotensin II type 1 receptor blocker; AT1, angiotensin II type 1 receptors; CKD, chronic kidney disease; DEPT, distortionless enhancement by polarization transfer; ECM, extracellular matrix; EMT, epithelial-to-mesenchymal transition; Fsp-1, fibroblast-specific protein 1; HSQC, heteronuclear single-quantum coherence; LEF, lymphoid enhancer-binding factor; MMP-7, matrix metalloproteinase-7; NOESY, nuclear overhauser effect spectroscopy; PAI-1, plasminogen activator inhibitor-1; PZC, poricoic acid ZC; PZD, poricoic acid ZD; PZE, poricoic acid ZE; qRT-PCR, quantitative real-time PCR; RAS, renin-angiotensin system; siRNA, small interfering RNA; SLPC, the surface layer of Poria cocos; TCF, T-cell factor; TGF-β, transforming growth factor-β; TGFβRI, transforming growth factor β receptor I; TGFβRII, transforming growth factor β receptor II; α-SMA, alpha smooth muscle actin.

■ REFERENCES

412 1. LeBleu, V. S.; Taduri, G.; O'Connell, J.; Teng, Y.; Cooke, V. G.; Woda, C.; Sugimoto, H.; Kalluri, R., Origin and
413 function of myofibroblasts in kidney fibrosis. *Nat Med* **2013**, *19*, 1047-1053.
414 2. Han, S. J.; Noh, M. R.; Jung, J. M.; Ishii, I.; Yoo, J.; Kim, J. I.; Park, K. M., Hydrogen sulfide-producing
415 cystathionine gamma-lyase is critical in the progression of kidney fibrosis. *Free radical biology & medicine* **2017**, *112*,
416 423-432.
417 3. Zhao, Y. Y.; Wang, H. L.; Cheng, X. L.; Wei, F.; Bai, X.; Lin, R. C.; Vaziri, N. D., Metabolomics analysis reveals
418 the association between lipid abnormalities and oxidative stress, inflammation, fibrosis, and Nrf2 dysfunction in
419 aristolochic acid-induced nephropathy. *Sci Rep* **2015**, *5*, 12936.
420 4. Jin, Y.; Ratnam, K.; Chuang, P. Y.; Fan, Y.; Zhong, Y.; Dai, Y.; Mazloom, A. R.; Chen, E. Y.; D'Agati, V.; Xiong,
421 H.; Ross, M. J.; Chen, N.; Ma'ayan, A.; He, J. C., A systems approach identifies HIPK2 as a key regulator of kidney
422 fibrosis. *Nat Med* **2012**, *18*, 580-8.
423 5. Wolf, G., Renal injury due to renin-angiotensin-aldosterone system activation of the transforming growth
424 factor-beta pathway. *Kidney Int* **2006**, *70*, 1914-1919.
425 6. Bottinger, E. P.; Bitzer, M., TGF-beta signaling in renal disease. *Journal of the American Society of Nephrology*
426 **2002**, *13*, 2600-2610.
427 7. Chen, D. Q.; Cao, G.; Chen, H.; Liu, D.; Su, W.; Yu, X. Y.; Vaziri, N. D.; Liu, X. H.; Bai, X.; Zhang, L.; Zhao, Y.
428 Y., Gene and protein expressions and metabolomics exhibit activated redox signaling and wnt/beta-catenin pathway are
429 associated with metabolite dysfunction in patients with chronic kidney disease. *Redox biology* **2017**, *12*, 505-521.
430 8. Chen, L.; Chen, D. Q.; Wang, M.; Liu, D.; Chen, H.; Dou, F.; Vaziri, N. D.; Zhao, Y. Y., Role of
431 RAS/Wnt/beta-catenin axis activation in the pathogenesis of podocyte injury and tubulo-interstitial nephropathy. *Chem*
432 *Biol Interact* **2017**, *273*, 56-72.

9. Xu, Z.; Li, W.; Han, J.; Zou, C.; Huang, W.; Yu, W.; Shan, X.; Lum, H.; Li, X.; Liang, G., Angiotensin II induces kidney inflammatory injury and fibrosis through binding to myeloid differentiation protein-2 (MD2). *Scientific Reports* **2017**, *7*, 44911.

10. Yang, F.; Huang, X. R.; Chung, A. C.; Hou, C. C.; Lai, K. N.; Lan, H. Y., Essential role for Smad3 in angiotensin II-induced tubular epithelial-mesenchymal transition. *The Journal of pathology* **2010**, *221*, 390-401.

11. Rodriguez-Vita, J.; Sanchez-Lopez, E.; Esteban, V.; Ruperez, M.; Egido, J.; Ruiz-Ortega, M., Angiotensin II activates the Smad pathway in vascular smooth muscle cells by a transforming growth factor-beta-independent mechanism. *Circulation* **2005**, *111*, 2509-17.

12. Remuzzi, G.; Perico, N.; Macia, M.; Ruggenenti, P., The role of renin-angiotensin-aldosterone system in the progression of chronic kidney disease. *Kidney international. Supplement* **2005**, S57-65.

13. Zhou, L.; Li, Y.; Hao, S.; Zhou, D.; Tan, R. J.; Nie, J.; Hou, F. F.; Kahn, M.; Liu, Y., Multiple genes of the renin-angiotensin system are novel targets of Wnt/beta-catenin signaling. *J Am Soc Nephrol* **2015**, *26*, 107-120.

14. Ai, J.; Nie, J.; He, J.; Guo, Q.; Li, M.; Lei, Y.; Liu, Y.; Zhou, Z.; Zhu, F.; Liang, M.; Cheng, Y.; Hou, F. F., GQ5 hinders renal fibrosis in obstructive nephropathy by selectively inhibiting TGF-beta-induced Smad3 phosphorylation. *J Am Soc Nephrol* **2015**, *26*, 1827-1838.

15. Zhao, Y. Y.; Chen, H.; Tian, T.; Chen, D. Q.; Bai, X.; Wei, F., A pharmaco-metabonomic study on chronic kidney disease and therapeutic effect of ergone by UPLC-QTOF/HDMS. *PLoS One* **2014**, *23*, e115467.

16. Ko, J.-W.; Shin, N.-R.; Park, S.-H.; Lee, I.-C.; Ryu, J.-M.; Kim, H.-J.; Cho, Y.-K.; Kim, J.-C.; Shin, I.-S., Silibinin inhibits the fibrotic responses induced by cigarette smoke via suppression of TGF-beta 1/Smad 2/3 signaling. *Food and Chemical Toxicology* **2017**, *106*, 424-429.

17. Zhao, Y. Y.; Zhang, L.; Mao, J. R.; Cheng, X. H.; R.C., L.; Zhang, Y.; Sun, W. J., Ergosta-4,6,8(14),22-tetraen-3-one isolated from Polyporus umbellatus prevents early renal injury in aristolochic acid-induced nephropathy rats. *J Pharm Pharmacol* **2011**, *63*, 1581-1586.

456 18. Zhao, Y. Y.; Cheng, X. L.; Cui, J. H.; Yan, X. R.; Wei, F.; Bai, X.; Lin, R. C., Effect of
457 ergosta-4,6,8(14),22-tetraen-3-one (ergone) on adenine-induced chronic renal failure rat: a serum metabonomic study
458 based on ultra performance liquid chromatography/high-sensitivity mass spectrometry coupled with MassLynx i-FIT
459 algorithm. *Clin. Chim. Acta* **2012**, *413*, 1438-1445.
460 19. Zhao, Y. Y.; Shen, X.; Cheng, X. L.; Wei, F.; Bai, X.; Lin, R. C., Urinary metabonomics study on the protective
461 effects of ergosta-4,6,8(14),22-tetraen-3-one on chronic renal failure in rats using UPLC Q-TOF/MS and a novel MSE
462 data collection technique. *Process Biochem* **2012**, *47*, 1980-1987.
463 20. Zhao, Y. Y.; Cheng, X. L.; Wei, F.; Bai, X.; Lin, R. C., Application of faecal metabonomics on an experimental
464 model of tubulointerstitial fibrosis by ultra performance liquid chromatography/high-sensitivity mass spectrometry with
465 MS(E) data collection technique. *Biomarkers* **2012**, *17*, 721-729.
466 21. Feng, Y. L.; Lei, P.; Tian, T.; Yin, L.; Chen, D. Q.; Chen, H.; Mei, Q.; Zhao, Y. Y.; Lin, R. C., Diuretic activity of
467 some fractions of the epidermis of Poria cocos. *J Ethnopharmacol* **2013**, *150*, 1114-1118.
468 22. Zhao, Y. Y.; Lei, P.; Chen, D. Q.; Feng, Y. L.; Bai, X., Renal metabolic profiling of early renal injury and
469 renoprotective effects of Poria cocos epidermis using UPLC Q-TOF/HSMS/MSE. *J Pharm Biomed Anal* **2013**, *81- 82*,
470 202-209.
471 23. Zhao, Y. Y.; Li, H. T.; Feng, Y. L.; Bai, X.; Lin, R. C., Urinary metabonomic study of the surface layer of Poria
472 cocos as an effective treatment for chronic renal injury in rats. *J Ethnopharmacol* **2013**, *148*, 403-410.
473 24. Zhao, Y. Y.; Feng, Y. L.; Bai, X.; Tan, X. J.; Lin, R. C.; Mei, Q., Ultra performance liquid chromatography-based
474 metabonomic study of therapeutic effect of the surface layer of Poria cocos on adenine-induced chronic kidney disease
475 provides new insight into anti-fibrosis mechanism. *PLoS One* **2013**, *8*, e59617.
476 25. Chen, D. Q.; Chen, H.; Chen, L.; Tang, D. D.; Miao, H.; Zhao, Y. Y., Metabolomic application in toxicity
477 evaluation and toxicological biomarker identification of natural product. *Chem Biol Interact* **2016**, *252*, 114-130.

26. Zhao, Y. Y.; Cheng, X. L.; Wei, F.; Bai, X.; Tan, X. J.; Lin, R. C.; Mei, Q., Intrarenal metabolomic investigation of chronic kidney disease and its TGF-beta1 mechanism in induced-adenine rats using UPLC Q-TOF/HSMS/MS(E). *J. Proteome Res.* **2013**, *12*, 2692–2703.

27. Chen, D. Q.; Chen, H.; Chen, L.; Vaziri, N. D.; Wang, M.; Li, X. R.; Zhao, Y. Y., The link between phenotype and fatty acid metabolism in advanced chronic kidney disease. *Nephrology, dialysis, transplantation : official publication of the European Dialysis and Transplant Association - European Renal Association* **2017**, *32*, 1154-1166.

28. Warrington, S. J.; Strutt, H.; Strutt, D., The Frizzled-dependent planar polarity pathway locally promotes E-cadherin turnover via recruitment of RhoGEF2. *Development* **2013**, *140*, 1045-1054.

29. Andl, T.; Le Bras, G. F.; Richards, N. F.; Allison, G. L.; Loomans, H. A.; Washington, M. K.; Revetta, F.; Lee, R. K.; Taylor, C.; Moses, H. L.; Andl, C. D., Concerted loss of TGFβ-mediated proliferation control and E-cadherin disrupts epithelial homeostasis and causes oral squamous cell carcinoma. *Carcinogenesis* **2014**, *35*, 2602-2610.

30. Cao, W.; Xu, J.; Zhou, Z. M.; Wang, G. B.; Hou, F. F.; Nie, J., Advanced oxidation protein products activate intrarenal renin-angiotensin system via a CD36-mediated, redox-dependent pathway. *Antioxidants & redox signaling* **2013**, *18*, 19-35.

31. Breyer, M. D.; Susztak, K., The next generation of therapeutics for chronic kidney disease. *Nature Reviews Drug Discovery* **2016**, *15*, 568-588.

32. He, W.; Tan, R. J.; Li, Y.; Wang, D.; Nie, J.; Hou, F. F.; Liu, Y., Matrix metalloproteinase-7 as a surrogate marker predicts renal Wnt/beta-catenin activity in CKD. *Journal of the American Society of Nephrology : JASN* **2012**, *23*, 294-304.

33. Kong, J.; Du, J.; Wang, Y.; Yang, M.; Gao, J.; Wei, X.; Fang, W.; Zhan, J.; Zhang, H., Focal adhesion molecule Kindlin-1 mediates activation of TGF-beta signaling by interacting with TGF-beta RI, SARA and Smad3 in colorectal cancer cells. *Oncotarget* **2016**, *7*, 76224-76237.

34. Tsukazaki, T.; Chiang, T. A.; Davison, A. F.; Attisano, L.; Wrana, J. L., SARA, a FYVE domain protein that recruits Smad2 to the TGFbeta receptor. *Cell* **1998**, *95*, 779-91.

35. Zhang, Z. H.; Vaziri, N. D.; Wei, F.; Cheng, X. L.; Bai, X.; Zhao, Y. Y., An integrated lipidomics and metabolomics reveal nephroprotective effect and biochemical mechanism of Rheum officinale in chronic renal failure. *Sci Rep* **2016**, *6*, 22151.

36. Zhang, Z. H.; Wei, F.; Vaziri, N. D.; Cheng, X. L.; Bai, X.; Lin, R. C.; Zhao, Y. Y., Metabolomics insights into chronic kidney disease and modulatory effect of rhubarb against tubulointerstitial fibrosis. *Sci Rep* **2015**, *5*, 14472.

37. Wang, M.; Chen, L.; Liu, D.; Chen, H.; Tang, D. D.; Zhao, Y. Y., Metabolomics highlights pharmacological bioactivity and biochemical mechanism of traditional Chinese medicine. *Chem Biol Interact* **2017**, *273*, 133-141.

38. Zhao, Y. Y., Metabolomics in chronic kidney disease. *Clin. Chim. Acta* **2013**, *422*, 59–69.

39. Cybulsky, A. V., Endoplasmic reticulum stress, the unfolded protein response and autophagy in kidney diseases. *Nat Rev Nephrol* **2017**, *advance online publication*.

40. Sun, Y. B.; Qu, X.; Caruana, G.; Li, J., The origin of renal fibroblasts/myofibroblasts and the signals that trigger fibrosis. *Differentiation; research in biological diversity* **2016**, *92*, 102-107.

41. Zhang, H.; Han, G. W.; Batyuk, A.; Ishchenko, A.; White, K. L.; Patel, N.; Sadybekov, A.; Zamlynny, B.; Rudd, M. T.; Hollenstein, K.; Tolstikova, A.; White, T. A.; Hunter, M. S.; Weierstall, U.; Liu, W.; Babaoglu, K.; Moore, E. L.; Katz, R. D.; Shipman, J. M.; Garcia-Calvo, M.; Sharma, S.; Sheth, P.; Soisson, S. M.; Stevens, R. C.; Katritch, V.; Cherezov, V., Structural basis for selectivity and diversity in angiotensin II receptors. *Nature* **2017**, *544*, 327-332.

42. Lichtnekert, J.; Kaverina, N. V.; Eng, D. G.; Gross, K. W.; Kutz, J. N.; Pippin, J. W.; Shankland, S. J., Renin-Angiotensin-Aldosterone System Inhibition Increases Podocyte Derivation from Cells of Renin Lineage. *Journal of the American Society of Nephrology : JASN* **2016**, *27*, 3611-3627.

43. Ruster, C.; Wolf, G., Renin-angiotensin-aldosterone system and progression of renal disease. *Journal of the American Society of Nephrology : JASN* **2006**, *17*, 2985-91.

44. Nusse, R.; Clevers, H., Wnt/beta-Catenin Signaling, Disease, and Emerging Therapeutic Modalities. *Cell* **2017**, *169*, 985-999.

45. Surendran, K.; Schiavi, S.; Hruska, K. A., Wnt-dependent beta-catenin signaling is activated after unilateral ureteral obstruction, and recombinant secreted frizzled-related protein 4 alters the progression of renal fibrosis. *Journal of the American Society of Nephrology : JASN* **2005**, *16*, 2373-84.

46. Xiao, L.; Zhou, D.; Tan, R. J.; Fu, H.; Zhou, L.; Hou, F. F.; Liu, Y., Sustained Activation of Wnt/beta-Catenin Signaling Drives AKI to CKD Progression. *J Am Soc Nephrol* **2016**, *27*, 1727-1740.

47. Lin, X.; Zha, Y.; Zeng, X. Z.; Dong, R.; Wang, Q. H.; Wang, D. T., Role of the Wnt/beta-catenin signaling pathway in inducing apoptosis and renal fibrosis in 5/6-nephrectomized rats. *Molecular medicine reports* **2017**, *15*, 3575-3582.

48. Meng, X. M.; Tang, P. M.; Li, J.; Lan, H. Y., TGF-beta/Smad signaling in renal fibrosis. *Frontiers in physiology* **2015**, *6*, 82.

49. Meng, X. M.; Huang, X. R.; Chung, A. C.; Qin, W.; Shao, X.; Igarashi, P.; Ju, W.; Bottinger, E. P.; Lan, H. Y., Smad2 protects against TGF-beta/Smad3-mediated renal fibrosis. *Journal of the American Society of Nephrology : JASN* **2010**, *21*, 1477-87.

50. Meng, X. M.; Nikolic-Paterson, D. J.; Lan, H. Y., TGF-beta: the master regulator of fibrosis. *Nat Rev Nephrol* **2016**, *12*, 325-338.

51. Xu, P.; Liu, J.; Derynck, R., Post-translational regulation of TGF-β receptor and Smad signaling. *FEBS Letters* **2012**, *586*, 1871-1884.

52. Vindevoghel, L.; Lechleider, R. J.; Kon, A.; de Caestecker, M. P.; Uitto, J.; Roberts, A. B.; Mauviel, A., SMAD3/4-dependent transcriptional activation of the human type VII collagen gene (COL7A1) promoter by transforming growth factor beta. *Proceedings of the National Academy of Sciences of the United States of America* **1998**, *95*, 14769-74.

53. Liu, F. Y.; Li, X. Z.; Peng, Y. M.; Liu, H.; Liu, Y. H., Arkadia regulates TGF-beta signaling during renal tubular epithelial to mesenchymal cell transition. *Kidney international* **2008**, *73*, 588-594.

54. Xie, F.; Zhang, Z.; van Dam, H.; Zhang, L.; Zhou, F., Regulation of TGF-beta Superfamily Signaling by SMAD Mono-Ubiquitination. *Cells* **2014**, *3*, 981-93.

568 **Figure legends**

569 **Figure 1. Novel triterpenoids from SLPC.** (A) Chemical structures of compounds PZF-PZH. (B) Key HMBC
570 correlations for compounds PZF-PZH. (C) Key NOESY correlations for compounds PZF-PZH.

571 **Figure 2. PZF, PZG and PZH attenuated TIF and podocyte injury induced by Ang II and TGF-β1.** (A)
572 Representative Western blot analyses revealed that the 10 μM of PZF, PZG and PZH exhibited stronger suppression of
573 TGF-β1-induced high expression of collagen I. (B) Representative Western blot analyses revealed that triterpene PZG
574 and PZH exhibited stronger suppression of TGF-β1-induced TIF in HK-2 cells, and diterpene PZF hardly reversed the
575 abnormality. (C) Graphic presentation of collagen I, fibronectin, α-SMA and E-cadherin expression in different groups
576 as indicated. (D) Representative Western blot analyses revealed that PZG and PZH performed better inhibitory effect on
577 Ang II-induced TIF in HK-2 cells, and diterpene PZF was weaker. (E) Graphic presentation of collagen I, fibronectin,
578 α-SMA and E-cadherin expression in different groups as indicated. (F) The abnormal mRNA expression of collagen I,
579 fibronectin, α-SMA and vimentin were decreased by PZG and PZH, while down-regulated E-cadherin was increased
580 after PZG and PZH stimulation. (G) Representative Western blot analyses revealed that PZG and PZH exhibited
581 powerful inhibitory effect of TGF-β1-induced podocyte injury, and PZF showed no inhibitory effect in MPC5. (H)
582 Graphic presentation of podocin, nephrin, podocalyxin and synaptopodin expression in different groups as indicated. (I)
583 Representative Western blot analyses revealed that PZG and PZH exhibited stronger suppression of podocyte injury
584 caused by Ang II, and PZF hardly reverse the injury in MPC5. (J) Graphic presentation of podocin, nephrin,
585 podocalyxin and synaptopodin expression in different groups as indicated. (K) Representative micrographs showed
586 vimentin expression in different groups in HK-2 cells. Each data represents the mean ± SD for groups of different
587 group. #P<0.05; ##P<0.01 versus CTL. *P<0.05; **P<0.01 versus TGF-β1 or Ang II stimulation.

588 **Figure 3. PZF, PZG and PZH inhibited the activation of RAS.** (A) Representative Western blot analyses revealed
589 that triterpene PZG and PZH down-regulated the activation of RAS in HK-2 cells after TGF-β1 stimulation, but
590 diterpene PZF showed no effect. (B) Graphic presentation of AGT, renin, ACE and AT1 expression in different groups

as indicated. (C) Representative Western blot analyses revealed that Ang II up-regulated the protein expression of RAS components, and PZG and PZH reversed the abnormal expression of AGT, renin, ACE and AT1 protein, but PZF performed no effect in HK-2 cells. (D) Graphic presentation of AGT, renin, ACE and AT1 expression in different groups as indicated. Each data represents the mean ± SD for groups of different group. #P<0.05; ##P<0.01 versus CTL. *P<0.05; **P<0.01 versus TGF-β1 or Ang II stimulation.

Figure 4. PZF, PZG and PZH suppressed activated Wnt/β-catenin and its downstream target genes expression. (A) Representative Western blot analyses demonstrated that triterpene PZG and PZH decreased activated Wnt/β-catenin and its downstream targets after TGF-β1 stimulation in HK-2 cells, but diterpene PZF showed no effect. (B) Graphic presentation of Wnt1, β-catenin, active β-catenin, snail, twist, MMP-7, PAI-1 and Fsp-1 expression in different groups as indicated. (C) Representative Western blot analyses showed that Ang II stimulated the accumulation of β-catenin and active β-catenin, and PZG and PZH decreased the abnormal expression of Wnt/β-catenin and its downstream targets, but PZF performed no effect in HK-2 cells. (D) Graphic presentation of Wnt1, β-catenin, active β-catenin, snail, twist, MMP-7, PAI-1 and Fsp-1 expression in different groups as indicated. (E) TGF-β1 up-regulated Wnt1, Wnt2, Wnt3, Wnt3a, Wnt7a and Wnt8a expression, and their abnormality were reversed after given PZG and PZH. (F) Representative micrographs showed β-catenin expression in different groups in HK-2 cells. (G) Representative Western blot analyses revealed that the inhibitory effect of PZG and PZH were obvious in TGF-β1-induced the activation of Wnt/β-catenin, but PZF showed no effect in MPC5. (H) Graphic presentation of Wnt1, β-catenin, active β-catenin, snail, twist, MMP-7, PAI-1 and Fsp-1 expression in different groups as indicated. (I) Representative Western blot analyses indicated that PZG and PZH reversed the abnormal expression of Wnt1, β-catenin, active β-catenin, snail, twist, MMP-7, PAI-1 and Fsp-1 protein caused by Ang II in MPC5, but PZF performed no effect in HK-2 cells. (J) Graphic presentation of Wnt1, β-catenin, active β-catenin, snail, twist, MMP-7, PAI-1 and Fsp-1 expression in different groups as indicated. Each data represents the mean ± SD for groups of different group. #P<0.05; ##P<0.01 versus CTL. *P<0.05; **P<0.01 versus TGF-β1 or Ang II stimulation.

614 **Figure 5. PZF, PZG and PZH selectively inhibits TGF-β1/Smad3 pathway.** (A) Representative Western blot
615 analyses showed that triterpene PZG and PZH exhibited stronger suppression of TGF-β1-induced up-regulation of
616 TGFβRI and p-Smad3 in HK-2 cells, and diterpene PZF hardly reversed the abnormality. (B) Graphic presentation of
617 TGFβRI, TGFβRII, p-Smad2, Smad2, p-Smad3, Smad3, Smad4 and Smad7 expression in different groups as indicated.
618 (C) Representative Western blot analyses revealed that PZG and PZH performed better inhibitory effect on Ang
619 II-induced high expression of TGFβRI and p-Smad3 in HK-2 cells, and diterpene PZF was weaker. (D) Graphic
620 presentation of TGFβRI, TGFβRII, p-Smad2, Smad2, p-Smad3, Smad3, Smad4 and Smad7 in different groups as
621 indicated. (E) Representative micrographs show p-Smad3 expression in different groups in HK-2 cells. (F)
622 Representative Western blot analyses indicated that PZG and PZH exhibited powerful inhibitory effect of
623 TGF-β1-induced activated TGF-β1/Smad3 pathway, and PZF showed no inhibitory effect in MPC5. (G) Graphic
624 presentation of TGFβRI, TGFβRII, p-Smad2, Smad2, p-Smad3, Smad3, Smad4 and Smad7 expression in different
625 groups as indicated. (H) Representative Western blot analyses demonstrated that PZG and PZH exhibited stronger
626 suppression of activated TGF-β1/Smad3 caused by Ang II, and PZF hardly reverse the injury in MPC5. (I) Graphic
627 presentation of TGFβRI, TGFβRII, p-Smad2, Smad2, p-Smad3, Smad3, Smad4 and Smad7 expression in different
628 groups as indicated. Each data represents the mean ± SD for groups of different group. #P<0.05; ##P<0.01 versus CTL.
629 *P<0.05; **P<0.01 versus TGF-β1 or Ang II stimulation.

630 **Figure 6. PZF, PZG and PZH selectively interrupt the interactions of Smad3 with TGFβRI and SARA in HK-2**
631 **cells.** (A) Representative Western blot analyses revealed that TGF-β1 enhanced the interactions of TGFβRI and
632 TGFβRII with Smad2 and Smad3, while PZF, PZG specifically broke the interaction between TGFβRI and Smad3, and
633 PZF showed no effect. (B) Graphic presentation of representative Western blot in different groups as indicated. (C)
634 Representative Western blot analyses demonstrated that PZF, PZG and PZH performed no effect on the connection of
635 Smad2 with TGFβRI and TGFβRII. (D) Graphic presentation of representative Western blot in different groups as
636 indicated. (E) Representative Western blot analyses revealed that apart from PZF, PZG and PZH owned powerful

inhibitory effect on the interactions of Smad3 with TGFβRI and TGFβRII. (F) Graphic presentation of representative Western blot in different groups as indicated. (G) Representative Western blot analyses indicated that PZF, PZG and PZH affected the interactions of SARA with TGFβRI and Smad3, but hardly changed the interaction of SARA with Smad2. (H) Graphic presentation of representative Western blot in different groups as indicated. (I) CO-IP demonstrated that PZG and PZH only influenced the interaction between SARA and Smad3. (J) Graphic presentation of representative Western blot in different groups as indicated. (K) PZG and PZH broke the interactions of SARA with TGFβRI and Smad3. Each data represents the mean ± SD for groups of different group. #P<0.05; ##P<0.01 versus CTL. *P<0.05; **P<0.01 versus TGF-β1 or Ang II stimulation.

Figure 7. PZF, PZG and PZH performed no anti-fibrotic effect after knockdown of Smad3. (A) Specific Smad3 siRNA evidently down-regulated protein expression of Smad3 in HK-2. Graphic presentation of β-catenin protein expression in different groups as indicated. (B) PZF, PZG and PZH had no effect on the RNAi of Smad3. Graphic presentation of β-catenin protein expression in different groups as indicated. (C) After knockdown Smad3, PZF, PZG and PZH performed no effect on renal fibrosis. (D) Graphic presentation of collagen I, fibronectin, α-SMA and E-cadherin expression in different groups as indicated. Each data represents the mean ± SD for groups of different group. #P<0.05; ##P<0.01 versus CTL. *P<0.05; **P<0.01 versus TGF-β1 or Ang II stimulation.

Figure 8. PZG and PZH inhibited EMT by suppressing the activation of RAS, Wnt/β-catenin and TGF-β1/Smad pathways. PZG and PZH selectively inhibited the phosphorylation of Smad3 to attenuate renal fibrosis. PZG and PZH suppressed the activation of RAS and performed like the combination of ACEI and ARB. PZG and PZH decreased Wnt1 and β-catenin protein expression.

660 **Table 1 Primers of Homo sapiens for qRT-PCR (5'→3') of EMT and Wnts genes**

Gene	Forward	Reverse	Product Size (bp)
Collagen I	TGTGCCACTCTGACTGGAAG	CGCCATACTCGAACTGGAATC	228
Fibronectin	CCACAGTGGAGTATGTGGTTAG	CAGTCCTTTAGGGCGATCAAT	104
α-SMA	GATGGTGGGAATGGGACAAA	GCCATGTTCTATCGGGTACTTC	94
Vimentin	GATTCACTCCCTCTGGTTGATAC	GTCATCGTGATGCTGAGAAGT	108
E-cadherin	CTTCTGCTGATCCTGTCTGATG	TGCTGTGAAGGGAGATGTATTG	144
Wnt1	CGGCGTTTATCTTCGCTATCA	GTAGTCACACGTGCAGGATT	95
Wnt2	CGGGAATCTGCCTTTGTTTATG	TTGGATCACAGGAACAGGATTT	103
Wnt3	CTGACTTCGGCGTGTTAGT	CCTCGTTGTTGTGCTTGTTC	93
Wnt3a	CAAGATTGGCATCCAGGAGT	ATGAGCGTGTCACTGCAAAG	173
Wnt7a	CGTGCTCAAGGACAAGTACA	GTACGACAGTGGCTTCTTGAT	103
Wnt8a	CAGTGAGAGCCACCATGAAA	CCTGGTCATACTTGGCCTTTAG	132
β-actin	ACAAGCCACAAGATTACAAG	ATCAGCAG TCTCATTCCAA	92

661

662

663

664

665

666

667

668 **Table 2 NMR data for PZF (500 MHz for ^{1}H and 125 MHz for ^{13}C, in pyridine)**

Position	C	H	HMBC (H to C)
1	39.0 (t)	1.51, 2.30 (m)	3, 4, 5, 10, 20
2	30.4 (d)	1.41 (m)	4, 10
3	35.3 (t)	2.54 (m)	4, 18, 19
4	48.0 (s)		
5	45.8 (d)	2.55 (m)	4, 7, 10, 18, 19, 21
6	19.4 (t)	1.63, 1.77 (m)	8, 18
7	30.8 (t)	2.88, 2.95 (m)	5, 8, 9, 14
8	135.5 (s)		
9	148.1 (s)		
10	37.6 (s)		
11	125.1 (d)	7.29 (d, J = 8.2 Hz)	3, 8, 10
12	124.7 (d)	7.12 (dd, J = 8.1, 1.8 Hz)	11, 13, 15
13	146.3 (s)		
14	127.7 (d)	6.95 (d, J = 1.3 Hz)	7, 9, 12, 15
15	34.3 (d)	2.81 (m)	12, 14
16	24.6 (q)	1.23 (s)	13, 15, 17
17	24.6 (q)	1.23 (s)	13, 15, 16
18	176.4 (s)		
19	17.5 (q)	1.49 (s)	3, 5, 1’
20	181.4 (s)		
21	25.7 (q)	1.21 (s)	1, 5, 10

1’	37.8 (t)	1.84, 2.08 (m)	19, 2’-6’
2’-6’	30.0 - 30.4 (t)	1.26 – 1.30	7’
7’	32.5 (t)	1.25	9’
8’	23.4 (t)	1.27	
9’	14.7 (q)	0.87 (m)	7’, 8’

669

670

671

672

673

674

675

676

677

678

679

680

681

682

683

684

685

686

687 **Table 3 NMR data for PZG and PZH (500 MHz for ^{1}H and 125 MHz for ^{13}C, in pyridine)**

Position	**PZG**		**PZH**	
	^{13}C	^{1}H	^{13}C	^{1}H
1	36.8 (t)	2.15, 1.93 (m)	33.1 (s)	1.73, 1.23 (m)
2	30.7 (t)	2.52 (dd, 10.7, 5.0)	23.8 (t)	2..30 (m)
3	177.0 (s)		77.4 (s)	4.60 (s)
4	149.7 (s)		42.8 (s)	
5	51.2 (d)	2.35 (s)	186.6 (s)	
6	28.9 (t)	2.56, 2.07 (m)	126.7 (d)	6.56 (s)
7	118.4 (d)	5.30 (t)	199.1 (s)	
8	142.3 (s)		140.1 (s)	
9	138.0 (s)		162.9 (s)	
10	39.3 (s)		43.6 (s)	
11	120.8 (d)	5.36 (br s)	30.3 (t)	1.27 (m)
12	37.5 (t)	2.71 (d, 17.9), 2.49 (m)	29.4 (t)	2.28, 2.13
13	46.0 (s)		46.9 (s)	
14	49.0 (s)		47.3 (s)	
15	44.1 (t)	2.43 (d, 8.7), 1.82 (m)	46.3 (t)	3.03, 2.96
16	76.8 (d)	4.53 (m)	76.1 (d)	4.48 (m)
17	58.0 (d)	2.87 (dd, 11.2, 6.0)	56.2 (d)	2.84 (m)
18	18.7 (q)	1.11 (s)	18.4 (q)	1.17 (s)
19	22.6 (q)	1.05 (s)	23.4 (q)	1.38 (s)
20	49.6 (d)	2.98 (dt, 11.2, 3.4)	49.0 (d)	2.96 (m)

21	179.2 (s)		179.5 (s)	
22	33.9 (t)	2.45 (m), 2.36 (s)	33.5 (t)	2.40, 2.54 (m)
23	23.8 (t)	2.10 (m), 1.89 (m)	23.8 (t)	2.30 (m)
24	45.3 (t)	1.85 (m), 1.72 (s)	156.4 (s)	
25	70.0 (s)		34.5 (d)	2.28 (m)
26	30.5 (q)	1.36 (s)	22.3 (q)	1.00 (s)
27	30.3 (q)	1.36 (s)	22.1 (q)	1.01 (s)
28	112.6 (t)	4.85, 4.78 (br s)	27.9 (q)	1.41 (s)
29	22.6 (q)	1.75 (s)	27.6 (q)	1.34 (s)
30	25.3 (q)	1.51 (s)	25.5 (q)	1.64 (s)
31			107.1 (t)	5.02, 4.87 (m)

688

689

690

691

692

693

694

695

696

697

698

699

Figure 1

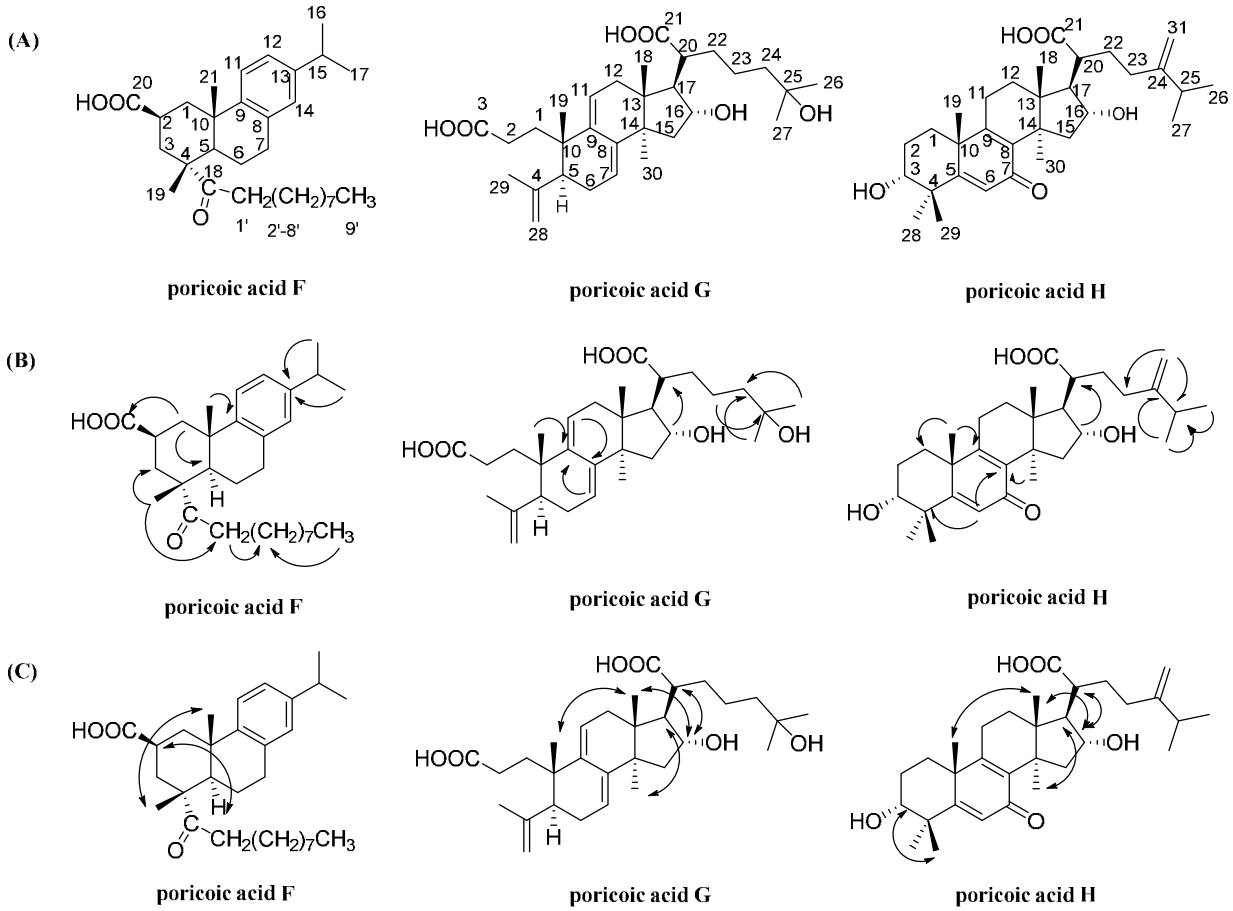
(A)
poricoic acid F
poricoic acid G
poricoic acid H
(B)
poricoic acid F
poricoic acid G
poricoic acid H
(C)
poricoic acid F
poricoic acid G
poricoic acid H

712 **Figure 2**

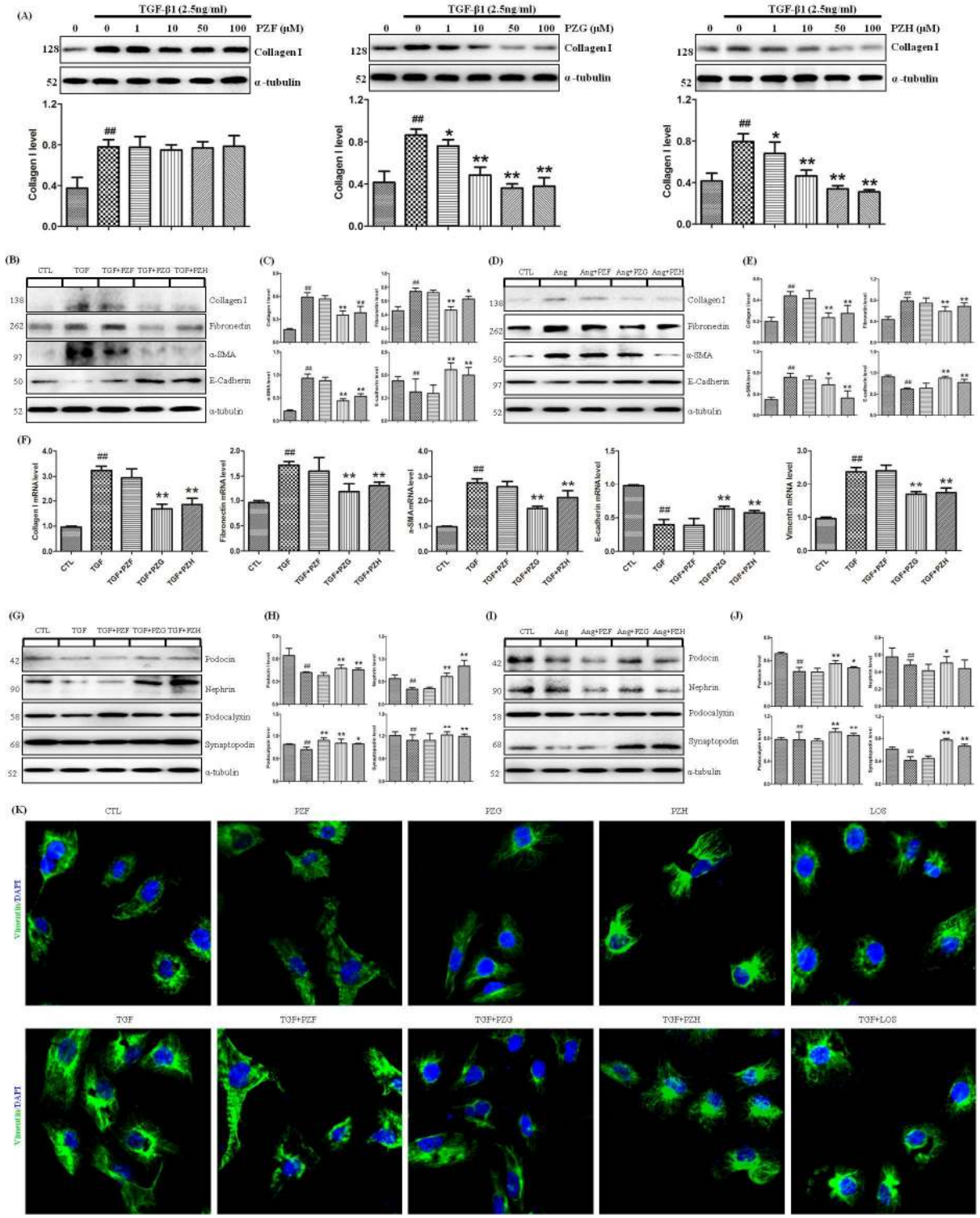

713

714

715

716

Figure 3

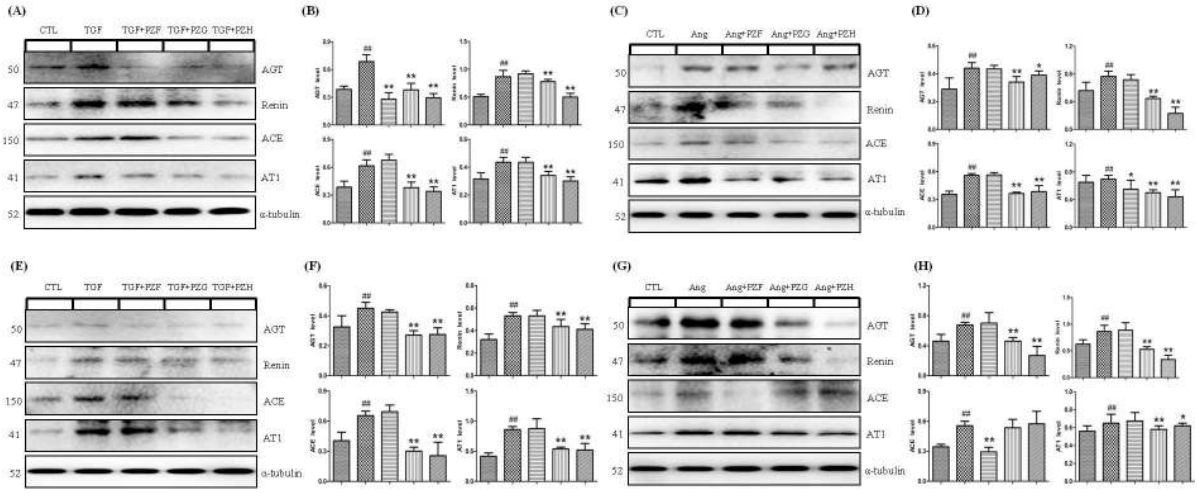
(A)
CTL
TGF
TGF+PZF
TGF+PZG
TGF+PZH
AGT
Renin
ACE
AT1
α-tubulin
(B)
(C)
CTL
Ang
Ang+PZF
Ang+PZG
Ang+PZH
(D)
(E)
(F)
(G)
(H)

735 **Figure 4**

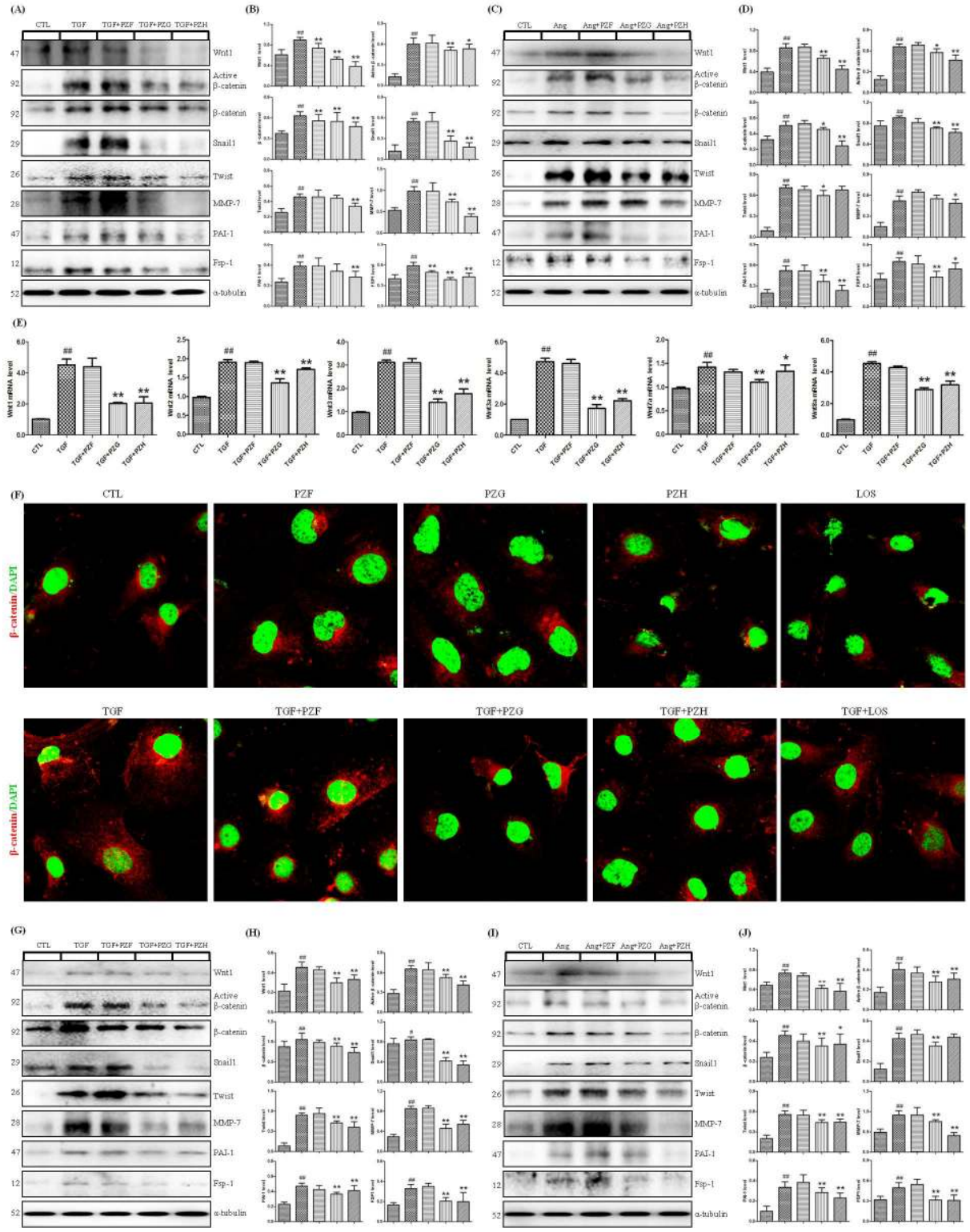

736

737

738

739 **Figure 5**

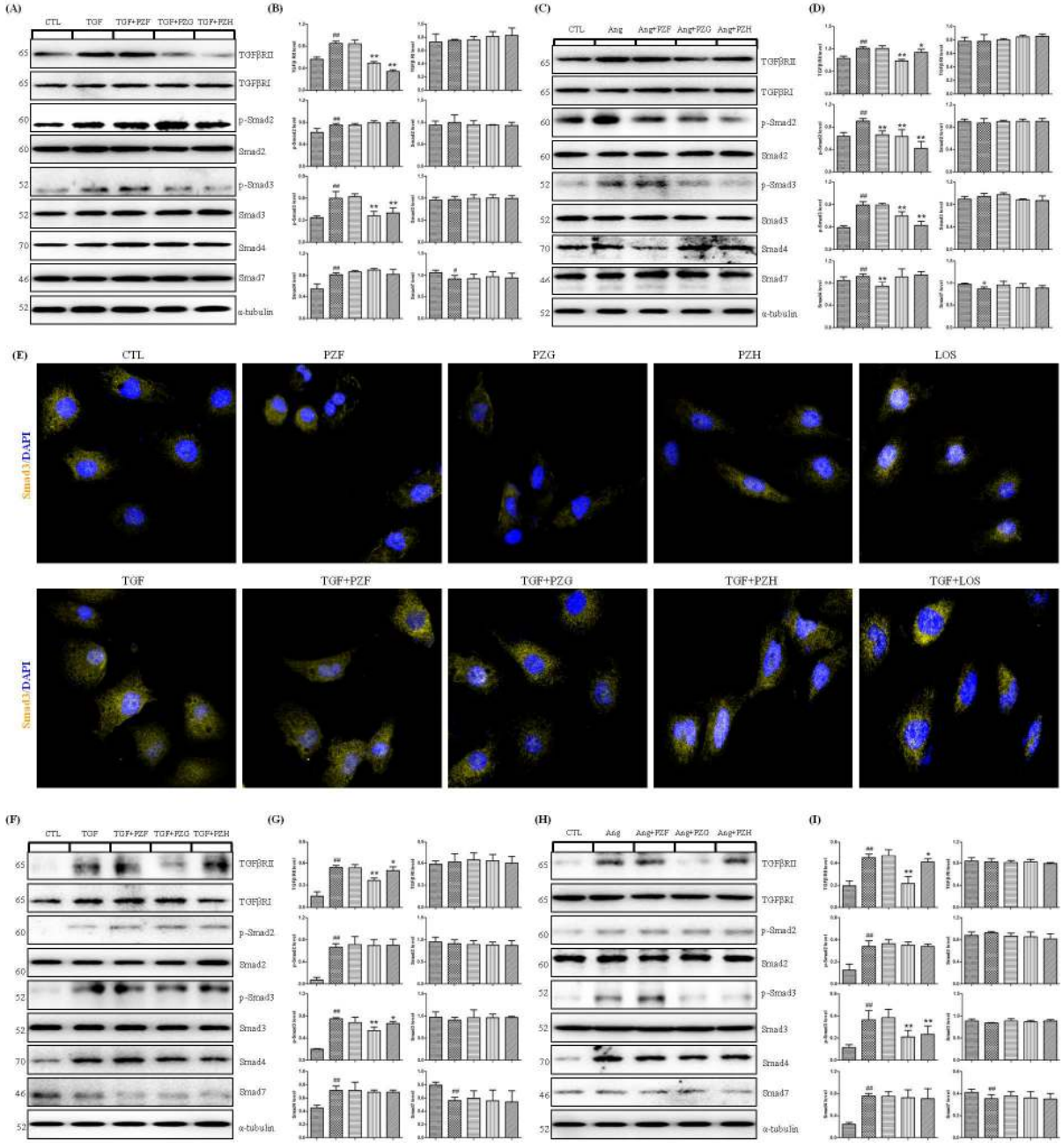

740

741

742

743

744

745

Figure 6

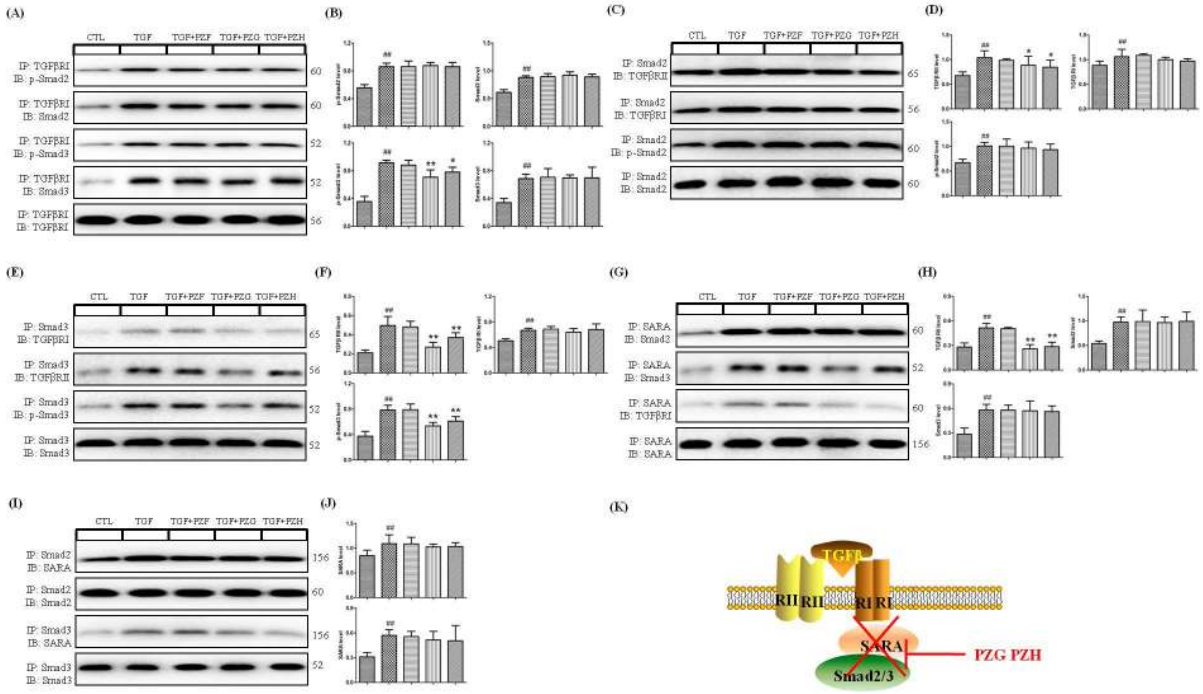
(A)
(B)
(C)
(D)
(E)
(F)
(G)
(H)
(I)
(J)
(K)
CTL
TGF
TGF+PZF
TGF+PZG
TGF+PZH
IP: TGFβRI IB: p-Smad2
IP: TGFβRI IB: Smad2
IP: TGFβRI IB: p-Smad3
IP: TGFβRI IB: Smad3
IP: TGFβRI IB: TGFβRI
IP: Smad2 IB: TGFβRII
IP: Smad2 IB: TGFβRI
IP: Smad2 IB: p-Smad2
IP: Smad2 IB: Smad2
IP: Smad3 IB: TGFβRI
IP: Smad3 IB: TGFβRII
IP: Smad3 IB: p-Smad3
IP: Smad3 IB: Smad3
IP: SARA IB: Smad2
IP: SARA IB: Smad3
IP: SARA IB: TGFβRI
IP: SARA IB: SARA
IP: Smad2 IB: SARA
IP: Smad3 IB: SARA
TGFβ
RII
RI
SARA
Smad2/3
PZG PZH

Figure 7

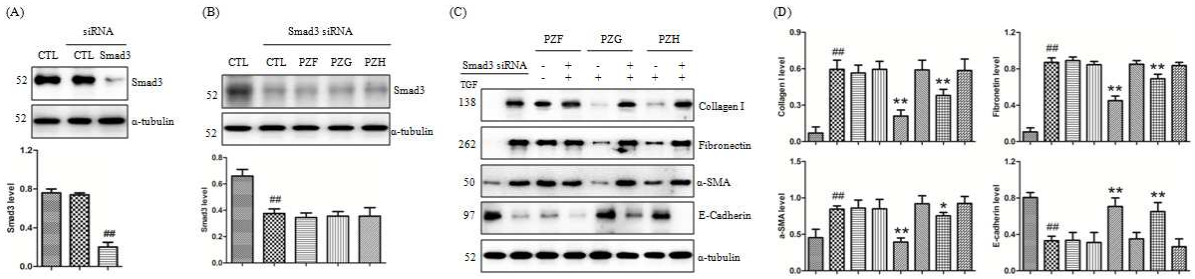
(A)
siRNA
CTL
CTL
Smad3
52
Smad3
52
α-tubulin
Smad3 level
##
(B)
Smad3 siRNA
CTL
CTL
PZF
PZG
PZH
52
Smad3
52
α-tubulin
Smad3 level
##
(C)
PZF
PZG
PZH
Smad3 siRNA
TGF
138
Collagen I
262
Fibronectin
50
α-SMA
97
E-Cadherin
52
α-tubulin
(D)
Collagen I level
Fibronectin level
α-SMA level
E-cadherin level
##
**
*

781 **Figure 8**

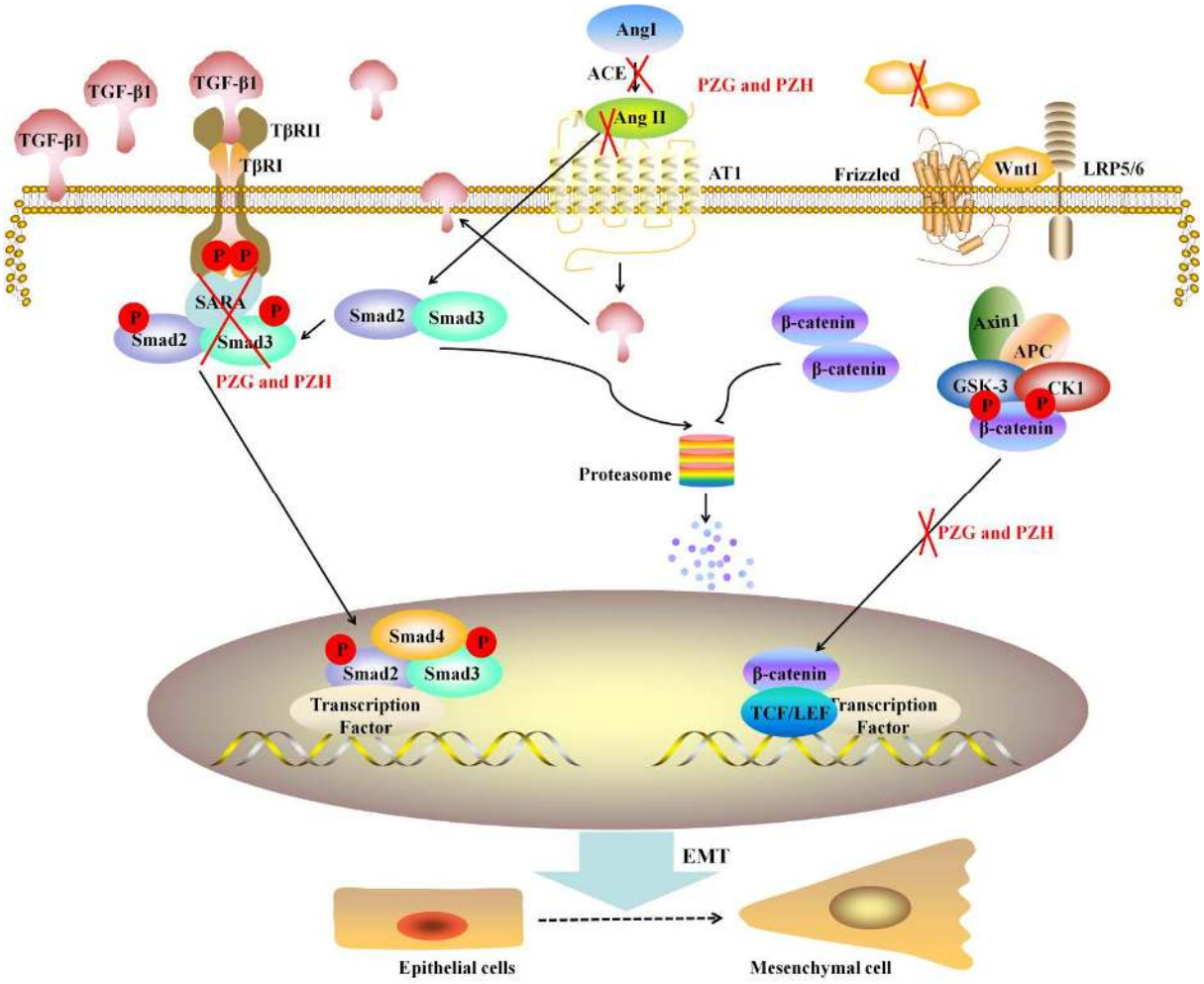

782

783

784

785

786

787

788

789

790

791

792 **TOC graphic**

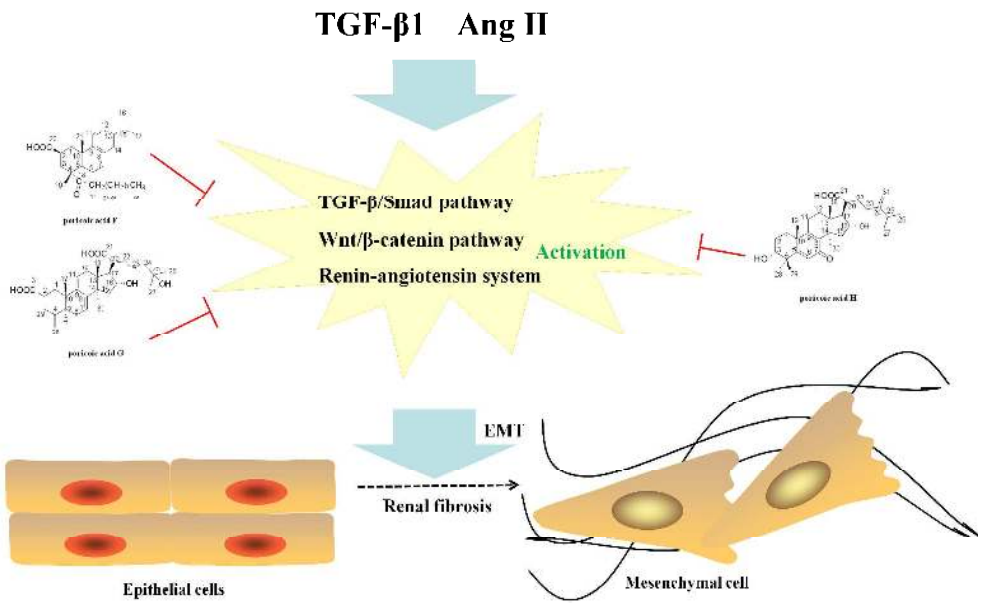

793

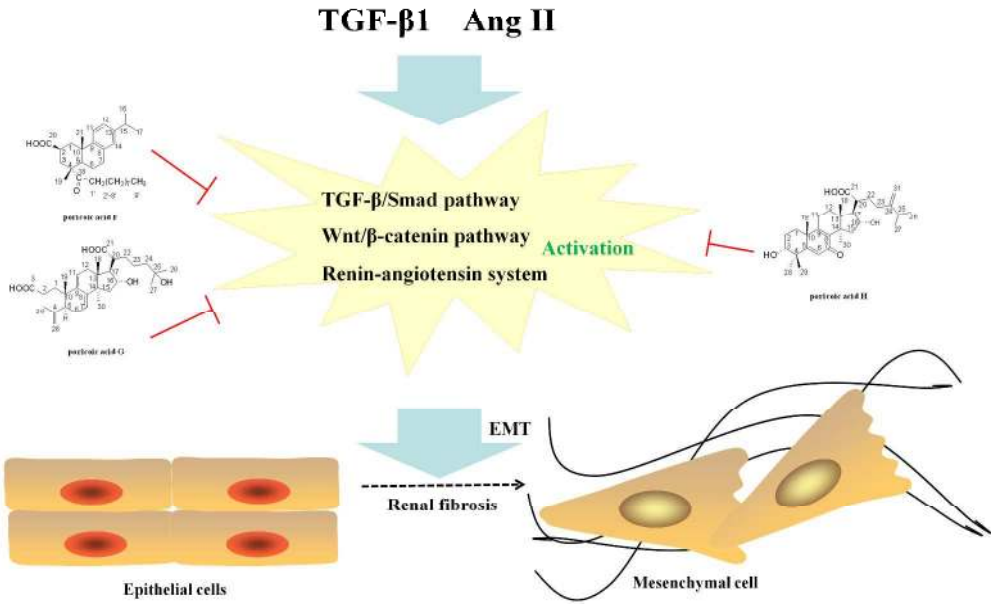

1021x693mm (96 x 96 DPI)